FREE VIBRATION OF FUNCTIONALLY GRADED MATERIAL PLATES USING FINITE ELEMENT ANALYSIS

Submitted By

TWISHA DEY

Class Roll No: 002011202023

Examination Roll No: M4MEC22023

Registration No: 154322 of 2020-21

Guided By

DR. TANMOY BANDYOPADHYAY

Department of Mechanical Engineering

JADAVPUR UNIVERSITY

KOLKATA – 700032

INDIA

2022

Faculty of Engineering & Technology

Jadavpur University

Kolkata-700 032

I hereby recommend that the thesis, entitled as — **"FREE VIBRATION OF FUNCTIONALLY GRADED MATERIAL PLATES USING FINITE ELEMENT ANALYSIS"**, prepared by Ms. Twisha Dey (Registration No-154322 of 2020-21) under my guidance, be accepted in partial fulfilment of the requirement for the degree of Master of Engineering (Applied Mechanics) from the Department of Mechanical Engineering of Jadavpur University.

Tanmoy Bandyopadhyay

21/06/2022

Adviser
Dr. Tanmoy Bandyopadhyay
Department of Mechanical Engineering
Jadavpur University

Assistant Professor
Dept. of Mechanical Engineering
Jadavpur University, Kolkata-32

Countersigned by:

Karmakar 21/06/2022

Prof. Amit Karmakar
Head
Department of Mechanical Engineering
Jadavpur University

Professor & Head
Dept. of Mechanical Engineering
Jadavpur University, Kolkata-32

Mazumdar 21/6/22

Prof. Chandan Mazumdar
Dean
FET
Jadavpur University

DEAN
Faculty of Engineering & Technology
JADAVPUR UNIVERSITY
KOLKATA-700 032

Faculty of Engineering & Technology

Jadavpur University

Kolkata-700 032

Certificate of Approval

*The foregoing thesis, entitled as "**FREE VIBRATION OF FUNCTIONALLY GRADED MATERIAL PLATES USING FINITE ELEMENT ANALYSIS**" is hereby approved by the committee of final examination for evaluation of thesis as a creditable study of an engineering subject carried out and presented by Ms. Twisha Dey (Registration No-154322 of 2020-21) in a manner satisfactory to warrant its acceptance as a perquisite to the degree of Master of Engineering (Mechanical Engineering). It is understood that by this approval, the undersigned do not necessarily endorse or approve any statement made, opinion expressed or conclusion drawn therein, but approve the thesis only for the purpose for which it is submitted.*

Committee of final examination for evaluation of thesis:

Dr. Tanmoy Bandyopadhyay
Assistant Professor & Supervisor
Mechanical Engg Department,
Jadavpur University

Dr. Amit Roy Chowdhury,
Professor & Head, External Examiner
Department of Aerospace Engg. & Applied Mechanics,
IIEST Shibpur

ACKNOWLEDGEMENT

It is a pleasant task to express my gratitude to all those who have assisted me in my project work.

First and foremost, I take this opportunity to express my sincere thanks and deepest sense of gratitude to my guide Dr. Tanmoy Bandyopadhyay, Department of Mechanical Engineering, for his continuous, valuable guidance, suggestions and encouragement throughout the project work, which helped me a lot to improve this project work. Their appreciation during the good times has been boosting my morals and confidence.

I express my heartiest thanks to all the faculty members of Mechanical Engineering and research scholars of 'Applied Mechanics' laboratory, Department of Mechanical Engineering, Jadavpur University for their support and encouragement during the research work.

I am indebted to Prof. Amit Karmakar, Head, Department of Mechanical Engineering, Jadavpur University, for his kind help during this project work.

I am also grateful to all the faculty members of Mechanical Engineering Department for their moral support, immense help and co-operation during the course of this thesis work.

I would like to express my heart-felt gratitude to my parents, my relatives and my friends for their love and active support throughout the endeavour.

Twisha Dey.

Date: 21/06/2022

Twisha Dey 21/06/'22

ABSTRACT

Functionally graded material (FGM) is an advanced composite material which have gained considerable importance in engineering applications in recent years. FGMs replaces the sharp transition of properties of conventional composite materials with smooth and continuous properties of the material such as physical, chemical, and mechanical like Young's Modulus, Poisson's ratio, Shear Modulus, density, and coefficient of thermal expansion in a desired spatial direction. The gradual changes in volume fraction of constituent and nonidentical structure at preferred direction give continuous graded properties like thermal conductivity, corrosion resistivity, specific heat, hardness, and stiffness ratio.

Two different materials such as metal and ceramic are mixed in FGM to obtain the coupled material properties of both materials. FGM plates are ceramic rich at the top surface, while the bottom surface is metal-rich. Toughness and strength are provided by metal, while thermal and corrosion resistance are obtained from ceramic. FGM has wide applications in in turbo-machinery, mechanical, aerospace, automobile and marine industries.

Turbo-machinery blades with low aspect ratio can be idealized as cantilever plates made of functionally graded material. In such application impact loading is applied during different stages of construction and service-life. Thus it is important to study the free vibration behaviour of the structure to ensure safety and reliability in operation. Accordingly, the present work is aimed at a finite element based analysis of the free vibration response of FGM plates.

An eight-noded isoparametric shell element is developed for the present finite element formulation. Different metal and ceramic combinations are considered for the FGM plates and the power law is employed to evaluate the material properties of FGM plate for different constituent combinations. The static equilibrium equations and the standard Eigen-value problem are solved by the QR iteration algorithm. The computer codes are utilized to generate numerical results.

TABLE OF CONTENTS

LIST OF FIGURES AND TABLES

Table 3.4(d) The first and the second natural frequencies of square Al/Al_2O_3 FGM plates for different twist angles (ψ) and power index values (k) for porosity type 3

Table 3.5(a) The first and the second natural frequencies of square $SUS304/Si_3N_4$ FGM plates for twist angles(ψ) and power index values(k) for no porosity (type 0)

Table 3.5(b) The first and the second natural frequencies of square $SUS304/Si_3N_4$ FGM plates for different twist angles (ψ) and power index values (k) for porosity type 1

Table 3.5(c) The first and the second natural frequencies of square $SUS304/Si_3N_4$ FGM plates for different twist angles (ψ) and power index values (k) for porosity type 2

Table 3.5(d) The first and the second natural frequencies of square $SUS304/Si_3N_4$ FGM plates for different twist angles (ψ) and power index values (k) for porosity type 3

Table 3.6(a) The first and the second natural frequencies of square Ti-6Al-4V/Aluminium Oxide FGM plates for different twist angles (ψ) and power index values (k) for no porosity (type 0)

Table 3.6(b) The first and the second natural frequencies of square Ti-6Al-4V/Aluminium Oxide FGM plates for different twist angles (ψ) and power index values (k) for porosity type 1

Table 3.6(c) The first and the second natural frequencies of square Ti-6Al-4V/Aluminium Oxide FGM plates for different twist angles (ψ) and power index values (k) for porosity type 2

Table 3.6(d) The first and the second natural frequencies of square Ti-6Al-4V/Aluminium Oxide FGM plates for different twist angles (ψ) and power index values (k) for porosity type 3

Table 3.7(a) The first and the second natural frequencies of square Al/ZrO_2 FGM plates for different twist angles(ψ) and power index values(k) for no porosity(type 0)

Table 3.7(b) The first and the second natural frequencies of square Al/ZrO_2 FGM plates for different twist angles(ψ) and power index values(k) for porosity type 1

Table 3.7(c) The first and the second natural frequencies of square Al/ZrO_2 FGM plates for different twist angles(ψ) and power index values(k) for porosity type 2

Table 3.7(d) The first and the second natural frequencies of square Al/ZrO_2 FGM plates for different twist angles(ψ) and power index values(k) for porosity type 3

Table 3.8(a) The first and the second natural frequencies of untwisted(ψ=0) Al/Al_2O_3 FGM plates for different aspect ratios(a/b) and power index values (k) for no porosity (type 0)

Table 3.8(b) The first and the second natural frequencies of untwisted(ψ=0) Al/Al_2O_3 FGM plates for different aspect ratios(a/b) and power index values (k) for porosity type 1

Table 3.8(c) The first and the second natural frequencies of untwisted(ψ=0) Al/Al_2O_3 FGM plates for different aspect ratios(a/b) and power index values (k) for porosity type 2

Table 3.8(d) The first and the second natural frequencies of untwisted(ψ=0) Al/Al_2O_3 FGM plates for different aspect ratios(a/b) and power index values (k) for porosity type 3

Table 3.9(a) The first and the second natural frequencies of untwisted(ψ=0) SUS304/Si_3N_4 FGM plates for different aspect ratios(a/b) and power index values (k) for no porosity (type 0)

Table 3.9(b) The first and the second natural frequencies of untwisted(ψ=0) SUS304/Si_3N_4 FGM plates for different aspect ratios*(a/b*) and power index values (k) for porosity type 1

Table 3.9(c) The first and the second natural frequencies of untwisted(ψ=0) SUS304/Si_3N_4 FGM plates for different aspect ratios(a/b) and power index values (k) for porosity type 2

Table 3.9(d) The first and the second natural frequencies of untwisted(ψ=0) SUS304/Si_3N_4 FGM plates for different aspect ratios(a/b) and power index values (k) for porosity type 3

Table 3.10(a) The first and the second natural frequencies of untwisted(ψ=0) Ti-6Al-4V/Aluminium Oxide FGM plates for different aspect ratios(a/b) and power index values (k) for no porosity (type 0)

Table 3.10(b) The first and the second natural frequencies of untwisted(ψ=0) Ti-6Al-4V/Aluminium Oxide FGM plates for different aspect ratios(a/b) and power index values (k) for porosity type 1

Table 3.10(c) The first and the second natural frequencies of untwisted(ψ=0) Ti-6Al-4V/Aluminium Oxide FGM plates for different aspect ratios(a/b) and power index values (k) for porosity type 2

Table 3.10(d) The first and the second natural frequencies of untwisted(ψ=0) Ti-6Al-4V/Aluminium Oxide FGM plates for different aspect ratios(a/b) and power index values (k) for porosity type 3

Table 3.11(a) The first and the second natural frequencies of untwisted(ψ=0) Al/ZrO_2 FGM plates for different aspect ratios(a/b) and power index values (k) for no porosity (type 0)

Table 3.11(b) The first and the second natural frequencies of untwisted(ψ=0) Al/ZrO_2 FGM plates for different aspect ratios(a/b) and power index values (k) for porosity type 1

Table 3.11(c) The first and the second natural frequencies of untwisted(ψ=0) Al/ZrO_2 FGM plates for different aspect ratios(a/b) and power index values (k) for porosity type 2

Table 3.11(d) The first and the second natural frequencies of untwisted(ψ=0) Al/ZrO_2 FGM plates for different aspect ratios(a/b) and power index values (k) for porosity type 3

Table 3.12(a) The first natural frequency values of untwisted(ψ=0) Al/Al_2O_3 FGM plates for different rotational speeds(ω) with varying power index values (k) and porosity types

CHAPTER - I

INTRODUCTION

1.1 GENERAL

1.1.1 *PREAMBLE*

With the advancement of modern technology composite materials have become an important class of materials due to their wide range of applications. Composites are highly advantageous because of their light weight, strength, design flexibility, and corrosion as well as wear resistance. The disadvantage of composites is they fail by delamination due to sharp transition of properties at the junction. To overcome this an advanced type of composite material named functionally graded materials (FGMs) was first proposed by the Japanese researchers for an aerospace project in 1984 **[1]**. The usefulness of functionally graded composites with a graded structure concept was previously recognized by **Shen and Bever** in 1972 **[2].**

FGMs are novel kinds of advanced composites which are primarily composed of metals at one surface and ceramics at the other. This is achieved by gradually varying the volume fraction of the constituent materials along the thickness. Thus, there is smooth transition of the material properties like Young's Modulus, Poisson's ratio, Shear Modulus, density, and coefficient of thermal expansion which relaxes the stress concentrations and delamination generally observed in layered structures. The metal part provides excellent strength and toughness, whereas the ceramic part imparts the ability to withstand high temperature environment. Therefore, FGMs have attracted the attention of a lot of researchers in the past few decades due to their potential application in spacecrafts, nuclear powerplants, automobile industries, biomedical equipment and other weight-sensitive applications.

Since this area is relatively new, industrial application and published literature on the behaviour of FGM plates is limited. But in general, FGM can be used in underwater vehicles, spacecrafts, leading edge of an aircraft wing, automobile bodies/protruded sections, blade of steam turbines and jet engines etc where the structures may experience variable environment. Turbo-machinery blades with low aspect ratio can be idealized as cantilever plates made of functionally graded material. So it is important to study the vibrational behaviour of the structure to ensure safety and reliability in operation. In present study, the free vibration characteristics of FGM cantilevered flat plate for different volume fractions, aspect ratio, porosity type and twist angle are demonstrated and discussed. To achieve this an eight-noded isoparametric shell element is developed for the present finite element formulation.

The power law is employed to evaluate the material properties of FGM plate at different points.

1.1.2 *TURBOMACHINERY BLADES*

The development of high-speed turbomachineries (i.e. turbines, compressors, fans and blowers) in the early 1950s resulted in the search for advanced materials that could resist the high temperature and the associated dynamic stress generated on the turbomachinery components. The failure of the turbine or turbo-compressor blades especially due to fatigue became a critical issue for researchers. The failure of the turbine blades was especially found to occur while vibrating near their resonant frequencies. As such, the accurate prediction of the natural frequencies of the turbomachinery blades became a topic of considerable research interest during the design phase itself. Owing to the fact that there are numerous fixed and rotating blades in a turbo-machine the accurate point of failure of such a system is extremely complex and hence requires very careful design.

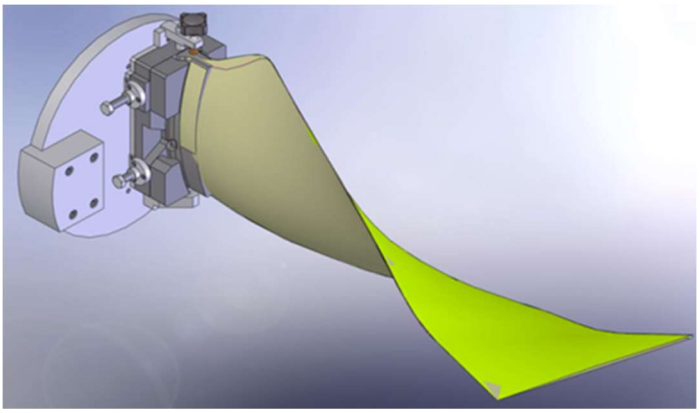

Figure 1.1. 3-dimensional view of a Turbomachinery twisted blade

1.1.3 *DYNAMIC BEHAVIOUR*

Blades are the vital part of a turbomachine since they are subjected to extreme dynamic loading during operation owing to rotation and random vibrations. The performance characteristics of these machines are largely dependent on the shape and geometry of the blades and hence their dynamic behavior is of considerable importance as far as the reliability and life of an engine is concerned. The major causes of failure of blades are fatigue in the lower temperature stages of a turbine or an axial flow compressor. In high temperature applications as in thermal power plants, the property degradation of composite blades leads to a reduction in their

strength and stiffness thereby leading to failure at much reduced loads. Blade failure due to fatigue is predominantly the consequence of resonant vibrations which gets aggravated at high temperatures. Such failures may be quite costly both in terms of safety and maintenance of turbine engines.

Although a turbine is designed to avoid resonance at its steady operating speed, it experiences resonance several times during the starting up and shutting down of the turbine. This may lead to shut down because of blade failure. In general, it is found that nearly all the vibrations of the blades are closely related to their natural frequencies. Thus, an in-depth knowledge of these frequencies is of fundamental importance to the designers in order to prevent vibration induced failures and ensure long life structurally sound blades.

However, an accurate prediction of these natural frequencies is usually very difficult because of the uncertainty of the excitation. It is equally difficult to predict the contribution of the complex blade geometries as well as the harmful effects of elevated temperature on such structures. The classic design practice for such blades has been mainly to rely on the blade natural frequencies to avoid harmful blade resonances. The natural frequencies are found by modelling the blades as cantilever plates and taking into account all the geometric complexities involved. The frequencies are determined at both stationary and rotating conditions taking into account the initial stresses resulting from rotation.

1.1.4 *FINITE ELEMENT METHOD*

The solution to the elasticity problems in the static and dynamic response of civil and aeronautical structures became much simplified with the introduction of high-speed computers in 1950s and 1960s. Finite element method (FEM) is a numerical technique to find approximate solutions of boundary value problems involving partial differential equations. This involves 4 discretization of the domain into various smaller sub-domains, known as finite elements, generating element equations for each of the finite elements, assembling the element equations of all the elements at specified nodes to generate the global equations which are then solved using appropriate solution techniques. The vibration of the composite shells involves many complex interactions between the shell structure, laminate properties, delamination behaviour, internal strains, initial stresses and impact of foreign bodies. The solution

of such problems is highly complex, computationally intensive and involves very large matrices. The availability of the modern high-speed computers and finite element software code NASTRAN along with the commercial software packages like ANSYS, ALGOR, COSMOS/M and ABACUS have been helpful in obtaining solution of problems in static and dynamic structural analysis, fluid flow, thermal analysis, electromagnetic and seismic response. The choice of a proper mathematical model, optimal discretization criteria and an appropriate solution technique is the prime requisite of any finite element simulation since it determines the closeness, reliability and its usability for modelling complex engineering applications.

1.1.5 *LIMITATIONS OF FEM*

The finite element method is an approximate technique and the accuracy of the simulation results are largely dependent on the choice of the finite elements used in the discretization process. The solution to the differential equations is obtained only at the nodal points and sometimes may not be representative of the response of an entire domain in case of complex geometries, irregularities in shape, curvature, unsymmetric stress distribution or non-linear behaviour. Thus, it becomes extremely essential to ascertain that the finite element modelling conforms to each and every aspect of a complex problem. The accuracy of the FEM method must also be thoroughly validated against experimental results incorporating numerous cycles of mesh enhancement/ refinement and error analysis until a required degree of precision is arrived at in what is known as an adaptive finite element analysis. In addition, most finite element simulations are computation intensive and may require large computation time and resources which must also be optimized for better design cycle time and cost reduction.

1.2. *LITERATURE REVIEW*

A literature review on the subject of free vibration of FGM structures discloses that researches on this topic are limited in the open literature. Bending, free vibration and buckling analyses of FGP micro-plates were conducted by Kim J. Kim, K.K. Zur, J.N. Reddy (2018) **[3]**. S. Coskun, J. Kim, and H. Toutanji implemented a general third-order plate theory to study bending, free vibration, and buckling of FG porous micro-plates (2019) **[4]**. Vibration characteristics of Functionally Graded shells and plates are studied by Loy, Lam & Reddy (2000) **[5]** and Zhao, Lee & Liew (2009) **[6]**. Nonlinear vibration and dynamic response of functionally graded plates in

thermal environments was studied by Huang and Shen (2004) **[7]**. Alijani, Bakhtiari-Nejad, Amabili also studied nonlinear vibrations of FGM rectangular plates in thermal environments (2011) **[8]**. Static and free vibration analysis of stiffened FGM plate was done by L.X. Peng et al. on elastic foundation based on physical neutral surface and MK method (2022) **[9]**. Free vibration of cracked FGM plates with variable thickness resting on elastic foundations was analysed by Phuc Pham Minh et al. (2021) **[10]**. The effect of cracks and thermal environment on free vibration of FGM plates was studied by Phuc Pham Minh and Nguyen Dinh Duc (2021) **[11]**.

There are a class of works dealing with the simulation of static and free vibration response of FGMs using the finite element method. For instance, static and free vibration analysis of FGM plates using an efficient quadrilateral finite element based on DSPM (2021). Gunes and Aydin (2010) **[12]** modelled the three-dimensional response of FGM media using the commercial finite element software. In that research an FGM circular plate was divided into a number of layers in the thickness direction, where each one was supposed as an isotropic homogeneous layer. Gunes et al. (2011) **[13]** developed their previous work for the case of elasto-plastic impact response of circular FGM plates. Mori-Tanaka scheme was applied to obtain the equivalent properties of each single layer. For the case of a sandwich beam with FGM core, Etemadi et al. (2009) **[14]** extended a three-dimensional simulation on the low velocity impact response of the structure.

To determine the free vibration characteristics stochastic finite element method was used by Xu Yalan et al. (2016) **[15]**. The low velocity impact response of FGM plates was studied by Larson and Palazotto (2009) **[16]** and Larson et al. (2006) **[17]** developed a combined experimental, computational and analytical method. In those investigations, a property estimation sequence was introduced for specifying the local elastic properties of a two-phased, two constituent FGM plate subjected to impact loading. It was indicated that the low velocity impact response of the plate based on FEM results were in good agreement with those obtained experimentally. To date, a few works have been studied on dynamic behaviour of plates made of functionally graded materials in two directions. Wirowski (2009) **[18]** studied free vibrations of thin annular plates made of a functionally graded material that is made of a two-phase functionally graded composite. The plate has a periodically inhomogeneous microstructure slowly varying along a circular coordinate, but smoothly graded properties in the radial direction. Also, Wirowski (2011, 2012) **[19,20]** analyzed the free vibration response of a thin rectangular plate band made

of a nonlinear functionally graded material. The material properties varied periodically in one direction and non-linearly in the other one. The effect of the material distribution on the overall response of the composite was studied.

There are only a few investigations related to the mathematical formulation of low velocity impact in FGMs. The main reason may be the contact force modelling between the projectile and target. Giannakopoulos and Suresh (1997) **[21]** studied the indentation of solids into a graded half-space. Two types of grading profiles, i.e., the exponential distribution and polynomial type of dispersion were considered in their works. In addition, the two-dimensional contact was also studied by Giannakopoulos and Pallot (2000) **[22]**. Those investigations may be useful to deduce the contact force expression for graded materials. For example, Mao et al. (2011) **[23]** analysed the response of a shallow spherical shell under the low velocity impact in a thermal field. The developed contact force formulation for the exponential property distribution revealed that the force-indentation relation in exponential FGMs was similar to the Hertz contact force, where force is proportional to $\alpha^{\frac{3}{2}}$. For media with transversely isotropic characteristics, Conway (1956) **[24]** and Turner (1980) **[25]** concluded a force-indentation relation through the Hertz contact force expression.

Such a character motivates the investigators to modify the Hertz contact force of finite thickness media in a way to account the graded profile through the thickness. For instance, Larson and Palazotto (2006) **[26]** developed a Hertzian type of the contact force in which the contact stiffness was modified to account the grading profile. The impact response of a circular FGM plate was analysed in their work. Shariyat and Jafari (2013) **[27]** obtained the low velocity impact behaviour of a circular plate with both radial and transverse graded profiles. In their work, symmetrical motion equations were obtained based on the first order shear deformation plate theory and the results were found via the Galerkin method.

In another study, Shariyat and Farzan (2013) **[28]** investigated the response of an FGM plate in rectangular shape under the eccentric impact. In that research, the first order shear deformation beam theory was used and the effect of in- -plane loads was also taken into consideration. Khalili et al. (2013) **[29]** studied the response of a thin FGM plate in rectangular shape that was subjected to low velocity impact. In another study, Dai et al. (2012) **[30]** studied the low velocity impact behaviour of shear deformable FGM circular plates. The solution in space and time domains was

obtained based on the orthogonal collocation point method and Newmark's method, respectively.

According to the above literature review, to date, the equivalent single-layer theories have been applied to analyse the low velocity impact response of FGM plates. Due to difficulty in obtaining solutions for low velocity impact analysis of FGM plates based on 3D elasticity, solutions are available only through a number of problems by the use of plate theories. Therefore, powerful numerical methods are needed to solve the governing equations. The graded finite element method (GFEM) is a relatively new numerical technique in structural analysis. Kim and Paulino (2002) **[31]**, and Zhang and Paulino (2007) **[32]**, developed a GFEM approach for modelling nonhomogeneous structures. In their studies, it was shown that the conventional FE formulations cause a discontinuous stress field in the direction perpendicular to the material property gradation, while the graded elements gave a continuous and smooth variation. Also, Asemi et al. (2012) **[33]** studied the dynamic response of thick short length FGM cylinders under an internal impact loading using the graded finite element method. Ashrafi et al. (2013) **[34]** presented a comparative study between the graded finite element and boundary element formulations capable of modelling nonhomogeneous behaviour of FGM structures.

A plenty of research is found to be carried out concerning the impact analysis of composite and FGM structures using different theories and models in the deterministic regime. Jam and Kiani (2015) **[35]** showed the effect of volume fraction of plate and temperature rise on contact force and contact time analysing FGM plates subjected to impact loading in thermal environment. Malekzadeh and Dehbozorgi (2016) **[36]** employed the first order shear deformation theory (FSDT), Hertzian nonlinear contact law and Mori–Tanaka model to investigate impact loading on plate displacement, impactor displacement, and contact force of FGM skew plate. Reddy's higher-order shear deformation theory along with element-free Ritz model is applied for impact analysis of nano-tube reinforced composite plates by Selim et al. (2017) **[37]**. Mata-Diaz et al. (2017) **[38]** carried out experimental investigations to 3 examine the effects of impact velocity on impact force and impact energy of composites. A comparative study between Auxetic Kevlar reinforced composites and standard Kevlar woven composites is carried out to investigate the structural behaviour under impact loading by Yang et al. (2017) **[39]**.

An impact analysis of plastic composite is conducted to probe the effect of impact velocity on impact energy and impact force by Liao and Liu (2017) **[40]**. Neogi et al. (2017) **[41]** carried out impact analysis of composite skewed hyper cell roofs subjected to impact loading with different impact velocity and impact angle along with anisotropic friction by using the finite element method (FEM). Coelho et al. (2017) **[42]** performed an experiment to investigate the performance of repaired composites (by over patch method) subjected to multiple impact loading. Experiments and numerical analyses are conducted on E-glass/epoxy-laminated composite for low impact analysis by Kursun et al. (2015) **[43]**. Modelling and experiments are executed for impact analysis of sandwich-structured composites with a honeycomb core by Chen et al. (2017) **[44]**. Kiani et al. (2013) **[45]** used third order shear deformation theory, the Hertz contact law, and fourth-order Runge–Kutta method to obtain low-velocity impact response of thick functionally graded material beam in a thermal environment.

Huang and Chen (2016) **[46]** carried out a comparative analysis of impact response between the powder metallurgy made FGM plate, multilayer composite, and pure composite revealing that delamination occurs in multi-layer composite, whereas it is found to be absent in FGM. Impact analysis of FGM truncated conical shell is carried out, when subjected to non-uniform buckling load by Zhang and Li (2010) **[47]**. Corrective Smoothed Particle Algorithm (CSPM) is utilised to high-velocity impact analysis of ceramic metal FGM plate by Eghtesad et al. (2012) **[48]**. Zhang and Zhang (2013) **[49]** applied the FEM method to optimise the design parameters such as thickness and density of each layer of FGM foam under impact loading. An FGM plate with finite crack subjected to impact loading is analysed for fracture behaviour of the plate by Ding and Li (2013) **[50]**. Damanpack et al. (2013) **[51]** analysed a sandwich beam to multiple low-velocity impact loading is analysed using the FEM. Shear-bending decomposition theory, the Mori–Tanaka model, and the Differential Quadrature Method (DQM) are used for impact analysis of viscoelastic functionally graded plates by Shariyat and Nasab (2014) **[52]**.Material modelling and numerical simulation are carried out for the impact analysis of fibre 4 reinforced composites using the Continuum Damage Mechanics (CDM) model by Johnson et al. (2001) **[53]**. Caputo et al. (2014) **[54]** a composite plate subjected to low-velocity impact loading is analysed by using numerical method, whereas an analytical method is employed for low velocity large mass impact analysis along with damage evolution of composite plate by Singh and Mahajan (2016) **[55]**.

CHAPTER - II

MATHEMATICAL FORMULATION

2.1 *FUNCTIONALLY GRADED MATERIAL PROPERTIES*

A functionally graded plate (shown in **Fig. 2.1**) is considered to be a single-layered plate of uniform thickness that is made of ceramic and metal. The material property is assumed to be graded through the thickness in accordance with a power-law distribution that is expressed as

$$P(z) = (P_c - P_m)\, V_c + P_m \,, \tag{2.1a}$$

$$V_c = \left(\frac{1}{2} + \frac{z}{h}\right)^k \qquad (k \geq 0)\,, \tag{2.1b}$$

where P represents the effective material property, P_c and P_m denote the properties of the ceramic and metal, respectively, V_c is the volume fraction of the ceramic, h is the thickness of the plate, and k is the volume fraction exponent.

A porosity distribution function $\psi(z)$ is defined

$$\begin{gathered}\psi(z) = \psi_{max} cos\left(\frac{\pi z}{h}\right) \\ \psi(z) = \psi_{max} cos\left[\frac{\pi}{2}\left(\frac{z}{h} + \frac{1}{2}\right)\right] \\ \psi(z) = \psi_{max} cos\left[\frac{\pi}{2}\left(\frac{z}{h} - \frac{1}{2}\right)\right]\end{gathered} \tag{2.2}$$

where, ψ_{max} is the maximum porosity and is expressed as a percentage. It is assumed to be $\psi_{max} = 0.50$ throughout the present study.

The graded material properties of a FGM shell are assumed to be based on the power law and accounts for the porosity distribution $\psi(z)$, expressed as

$$E(z) = \left\{(E_C - E_M) * \left[\frac{1}{2} + \left(\frac{z}{h}\right)\right]^k + E_M\right\} \times (1 - \psi(z)) \tag{2.3a}$$

$$\rho(z) = \left\{(\rho_C - \rho_M) * \left[\frac{1}{2} + \left(\frac{z}{h}\right)\right]^k + \rho_M\right\} \times (1 - \psi(z)) \tag{2.3b}$$

$$\nu(z) = \left\{(\nu_C - \nu_M) * \left[\frac{1}{2} + \left(\frac{z}{h}\right)\right]^k + \nu_M\right\} \times (1 - \psi(z)) \tag{2.3c}$$

$$\alpha(z) = \left\{(\alpha_C - \alpha_M) * \left[\frac{1}{2} + \left(\frac{z}{h}\right)\right]^k + \alpha_M\right\} \times (1 - \psi(z)) \tag{2.3d}$$

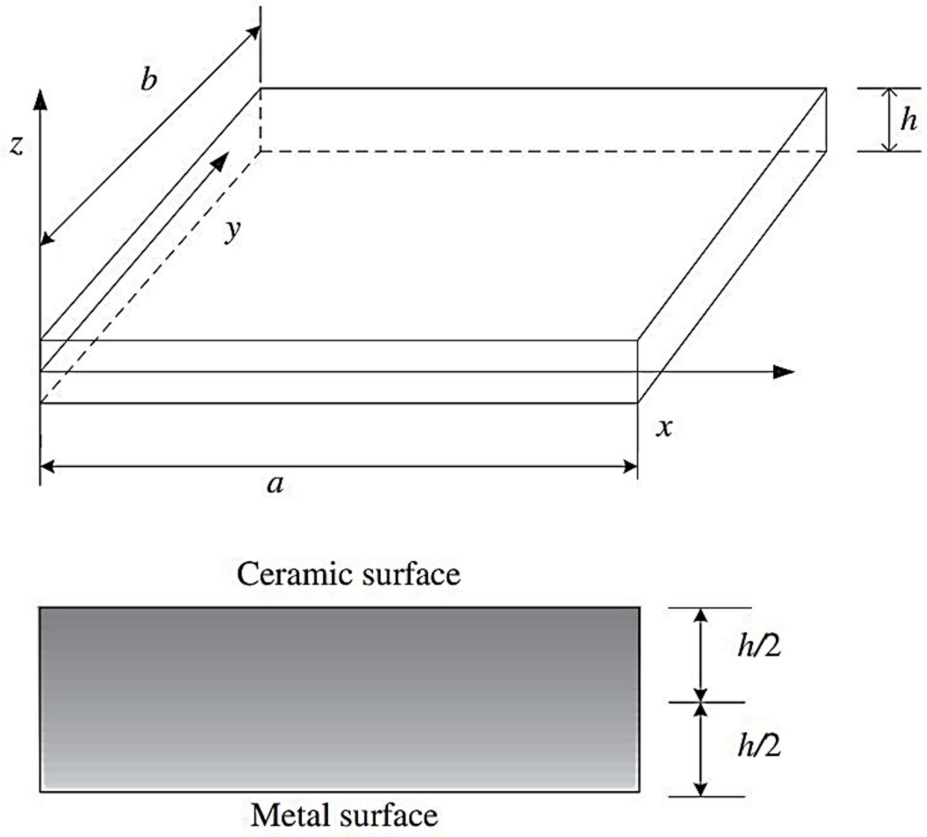

Fig 2.1. Functionally Graded Plate

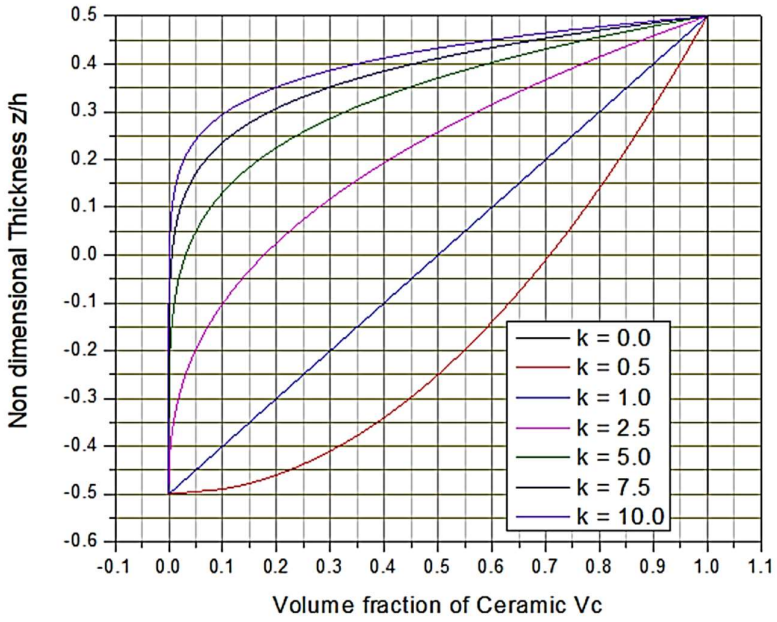

Fig 2.2. Variation of the volume fraction V_c through thickness

Fig. 2.2 shows the variation of the volume fraction through the thickness for different exponents k. The effective material properties of the plate, including Young's modulus E, density ρ, Poisson ratio ν, and thermal expansion β, vary according to Eq. (1). The properties of the temperature-dependent constituents of FGPs, such as Ti–6Al–4V, Silicon Nitride (Si_3N_4) and stainless steel (SUS304), can be expressed as a nonlinear function of temperature as

$$P = P_0(P_{-1}T^{-1} + 1 + P_1T + P_2T^2 + P_3T^3)\,, \tag{2.4}$$

where P_0, P_1, P_2, and P_3 are the coefficients of temperature T.

2.2 *GOVERNING EQUATIONS FOR A LAMINAR STRUCTURE*

The FGM structure may be assumed to be consisting of different layers rigidly bonded together such that each layer has its material properties as intermediate between the metal and ceramic constituent present at the bottom and top layers respectively. Each such lamina may be assumed to be isotropic with the properties being calculated at the mid-plane of the layer. The number of such lamina comprising the FGM may be obtained by performing convergence studies which such that the layered analysis may yield accurate results regarding the free vibration behavior of the FGM structure as a whole. The present analysis is

carried out considering the FGM plate to be comprising of 10 such constituting layers based on convergence studies.

The basic behavior of a unidirectional lamina as shown in **Fig 2.3** is assumed to be linearly elastic. The most common form of expressing the stress- strain relations of an orthotropic lamina involve plane stress conditions and engineering constants.

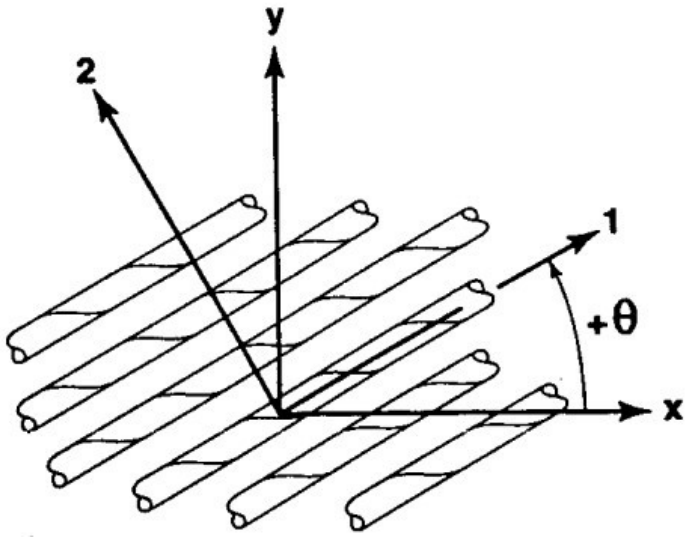

Fig 2.3. An arbitrary oriented laminate

(Positive rotation of principal material axes from x-y axes [56])

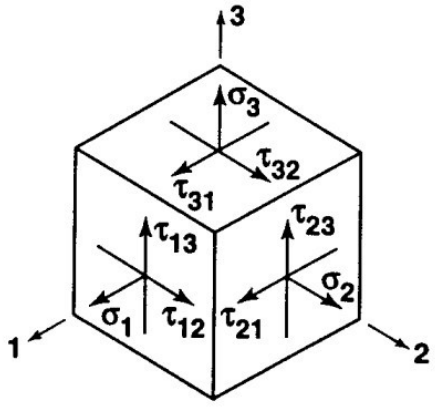

Fig 2.4. Stresses on an element

Neglecting the normal stress perpendicular to the plate of the lamina, the stress-strain relations, in the principal material direction 1, 2 and 3 (**Fig 2.2**) are given by

$$\begin{bmatrix} \sigma_1 \\ \sigma_2 \\ \tau_{12} \end{bmatrix} = \begin{bmatrix} Q_{11} & Q_{12} & 0 \\ Q_{12} & Q_{22} & 0 \\ 0 & 0 & Q_{66} \end{bmatrix} \begin{bmatrix} \varepsilon_1 \\ \varepsilon_2 \\ \varepsilon_3 \end{bmatrix} \tag{2.5a}$$

$$\begin{bmatrix} \tau_{13} \\ \tau_{23} \end{bmatrix} = \begin{bmatrix} Q_{44} & 0 \\ 0 & Q_{55} \end{bmatrix} \begin{bmatrix} \gamma_{13} \\ \gamma_{23} \end{bmatrix} \tag{2.5b}$$

Where,

$$Q_{11} = E_1 / (1-\nu_{12}\nu_{21})$$

$$Q_{12} = \nu_{12}E_2/ (1- \nu_{12}\nu_{21})$$

$$Q_{22} = E_2/ (1- \nu_{12}\nu_{21}) \tag{2.6}$$

$$Q_{66}=G_{12},\ Q_{44}=G_{13},\ Q_{55}=G_{23}$$

The stress-strain relations of the lamina, with respect to the x, y and z axes (**Fig 2.3**), are expressed as

$$\begin{bmatrix} \sigma_x \\ \sigma_y \\ \sigma_{xy} \end{bmatrix} = \left[\bar{Q}\right] \begin{bmatrix} \varepsilon_x \\ \varepsilon_y \\ \varepsilon_{xy} \end{bmatrix} = \begin{bmatrix} \bar{Q}_{11} & \bar{Q}_{12} & \bar{Q}_{16} \\ \bar{Q}_{12} & \bar{Q}_{22} & \bar{Q}_{26} \\ \bar{Q}_{16} & \bar{Q}_{26} & \bar{Q}_{66} \end{bmatrix} \begin{bmatrix} \varepsilon_x \\ \varepsilon_y \\ \varepsilon_{xy} \end{bmatrix} \tag{2.7a}$$

$$\begin{bmatrix} \tau_{xz} \\ \tau_{yz} \end{bmatrix} = \begin{bmatrix} \bar{Q}_{44} & \bar{Q}_{45} \\ \bar{Q}_{45} & \bar{Q}_{55} \end{bmatrix} \begin{bmatrix} \gamma_{xz} \\ \gamma_{yz} \end{bmatrix} \tag{2.7b}$$

Where

$\overline{Q_{11}} = Q_{11}Cos^4\theta + 2(Q_{12} + 2Q_{66})Sin^2\theta\, Cos^2\theta + Q_{22}Sin^4\theta,$

$\overline{Q_{12}} = (Q_{11}Q_{22} - 4Q_{66})Sin^2\theta Cos^2\theta + Q_{12}(Sin^4\theta + Cos^4\theta),$

$\overline{Q_{22}} = Q_{11}Sin^4\theta + 2(Q_{12} + 2Q_{66})\, Sin^2\theta Cos^2\theta + Q_{22}Cos^4\theta,$

$\overline{Q_{16}} = (Q_{11} - Q_{12} - 2Q_{66})Sin\theta Cos^3\theta + (Q_{12} - Q_{22} + 2Q_{66})Sin^3\theta Cos\theta$

$\overline{Q_{26}} = (Q_{11} - Q_{12} - 2Q_{66})Sin^3\theta Cos\theta + (Q_{12} - Q_{22} + 2Q_{66})Sin\theta Cos^3\theta$

$\overline{Q_{66}} = (Q_{11} + Q_{22} - 2Q_{12} - 2Q_{66})Sin^2\theta Cos^2\theta + Q_{66}(Sin^4\theta + COs^4\theta)$

$\overline{Q_{44}} = Q_{44}Cos^2\theta + Q_{55}Sin^2\theta$

$\overline{Q_{45}} = (Q_{55} - Q_{44})Sin\theta Cos\theta$

$\overline{Q_{55}} = Q_{55}Cos^2\theta + Q_{44}Sin^2\theta$

(2.8)

2.3 *FINITE ELEMENT STRUCTURAL ANALYSIS*

A laminated plate (**Fig. 2.5**) can be regarded as consisting of unidirectional laminate bonded together to act as an integral part. The bonds are infinitesimally thin and are non-shear deformable. Hence, the displacements are continuous throughout the thickness of the laminate. The following assumptions are made according to the Yang-Norris-Stavasky theory [57] which is a generalization of the Mindlin's theory to laminated plates.

- The deflection of the laminated plate is small.
- Normal to the mid surface before deformation remains straight but is not necessarily after deformation.
- Stresses normal to the mid surface are neglected.

The analysis is made by considering a laminated plate as considered in **Fig. 2.5**. The layer details of the laminate are shown in **Fig. 2.6**.

The in-plane displacements of a plate u and v of any point at a distance z from the mid-surface are given by

$$u(x, y, z, t) = u^0(x, y, t) + z\theta_y(x, y, t)$$

$$v\,(x, y, z, t) = v^0\,(x, y, t) - z\theta_x(x, y, t)$$

$$w\,(x, y, z, t) = w^0(x, y, t)$$

(2.9)

Where, u, v and w are displacements in x, y and z directions, respectively, and the superscript (^{0}) corresponds to the mid-plane values. Here, θ_x and θ_y denote the rotations of the cross-sections perpendicular to the x- and y-axis respectively.

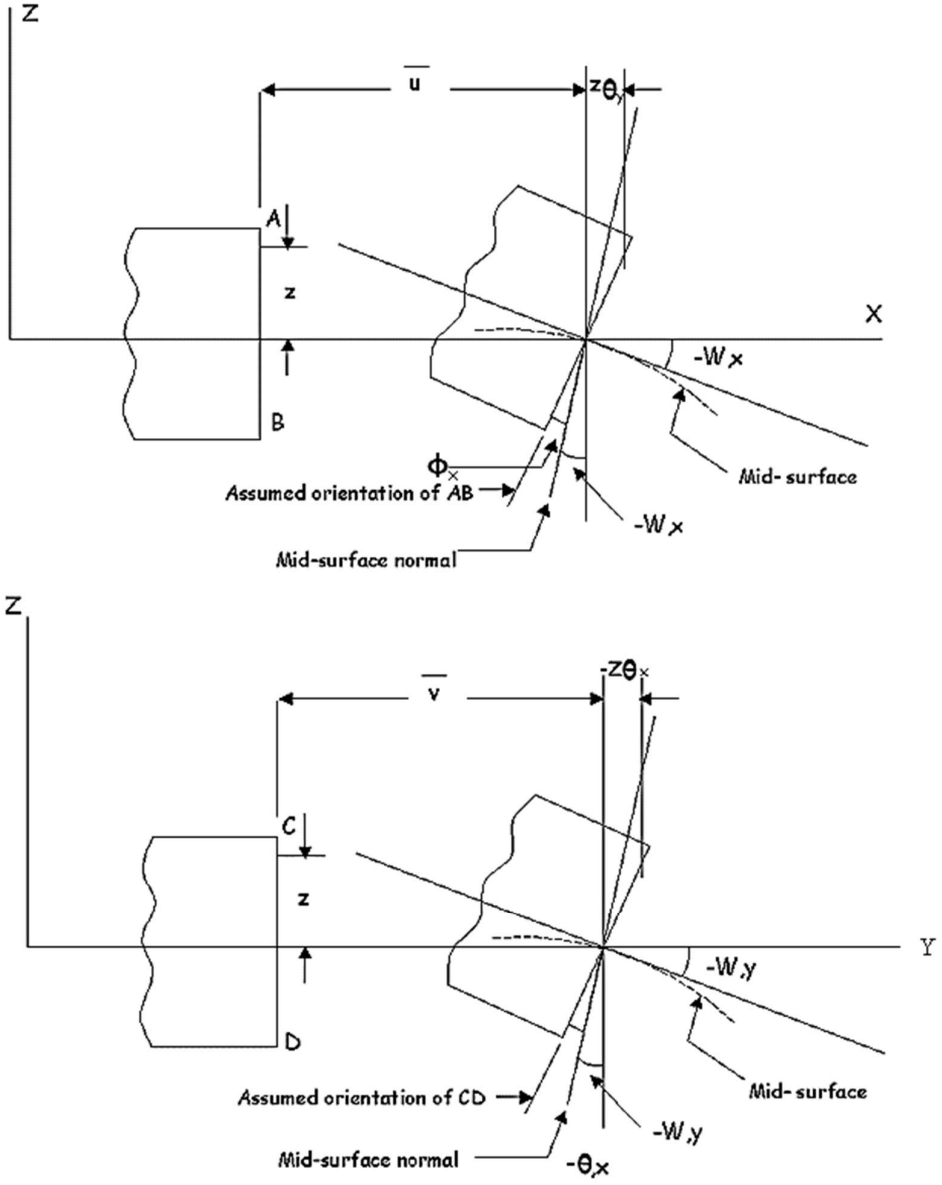

Fig 2.5. Plate deformation

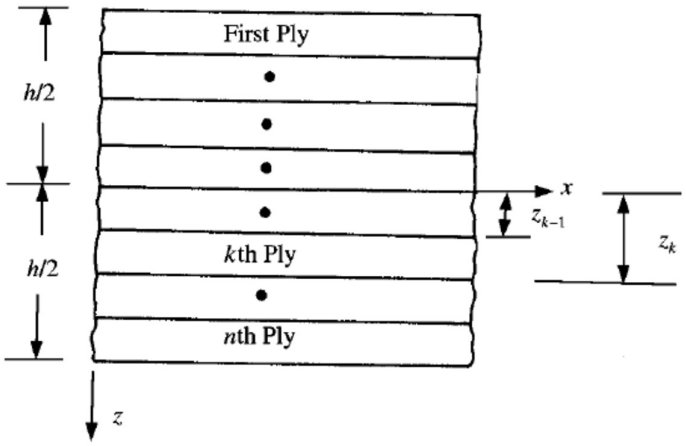

Fig 2.6. A typical laminate with layer details

Again, the shear rotations of the plate can be expressed as

$$\phi_x = \theta_y + w_{,x}\,, \quad \phi_y = -\,\theta_x + w_{,y} \tag{2.10}$$

The linear in-plane strains of the laminate at a distance z from the mid surface are given by

For plates,

$$\varepsilon_x = \frac{\partial u}{\partial x} = u_{,x} = \frac{\partial u^0}{\partial x} + z\frac{\partial \theta_y}{\partial x} = u^0_{,x} + z\theta_{y,x}$$

$$\varepsilon_y = \frac{\partial v}{\partial y} = v_{,y} = \frac{\partial v}{\partial y} - z\frac{\partial \theta_x}{\partial y} = v^0_{,y} - z\theta_{x,y}$$

$$\gamma_{xy} = u_{,y} + v_{,x} = u^0_{,y} + v^0_{,x} + z(\theta_{y,y} - \theta_{x,x})$$

(2.11)

The above equations can be expressed as

For plates,

$$\begin{bmatrix} \varepsilon_x \\ \varepsilon_y \\ \gamma_{xy} \end{bmatrix} = \begin{bmatrix} \varepsilon^0_x \\ \varepsilon^0_y \\ \gamma^0_{xy} \end{bmatrix} + z \begin{bmatrix} k_x \\ k_y \\ k_{xy} \end{bmatrix}$$

(2.12)

Now

$$\begin{bmatrix} \varepsilon_x^0 \\ \varepsilon_x^0 \\ \gamma_{xy}^0 \end{bmatrix} = \begin{bmatrix} u_{,x}^0 \\ v_{,y}^0 \\ u_{,y}^0 + v_{,x}^0 \end{bmatrix} \tag{2.13}$$

$$\begin{bmatrix} k_x \\ k_y \\ k_{xy} \end{bmatrix} = \begin{bmatrix} \theta_{y,x} \\ -\theta_{x,y} \\ \theta_{y,y} - \theta_{x,x} \end{bmatrix} \tag{2.14}$$

Since the transverse shear deformation is assumed same across the thickness of the laminate, γ_{xz} and γ_{yz} are identical to ϕ_x and ϕ_y, respectively

$$\gamma_{xz} = \phi_x, \gamma_{yz} = \phi_y \tag{2.15}$$

Substituting Eqn. in equations (2.3) and (2.4),

From, Eq. (2.5a) and (2.5b), the stresses in the k[th] lamina (**Fig 2.6**) of a multilayered laminate can be expressed as

$$\{\sigma\}_k = [\bar{Q}]_k \{\varepsilon\}_k \tag{2.16}$$

By substitution of the strain variation through the thickness, Eq. 2.8, in the stress-strain relations, Eq. 2.13, the stresses in the k[th] layer can be expressed in terms of the laminate middle-surface strains and curvature as

$$\begin{bmatrix} \sigma_x \\ \sigma_y \\ \tau_{xy} \end{bmatrix}_k = \begin{bmatrix} \bar{Q}_{11} & \bar{Q}_{12} & \bar{Q}_{16} \\ \bar{Q}_{12} & \bar{Q}_{22} & \bar{Q}_{26} \\ \bar{Q}_{16} & \bar{Q}_{26} & \bar{Q}_{66} \end{bmatrix}_k \left[\begin{bmatrix} \varepsilon_x^0 \\ \varepsilon_y^0 \\ \gamma_{xy}^0 \end{bmatrix} + z \begin{bmatrix} \kappa_x \\ \kappa_y \\ \kappa_{xy} \end{bmatrix} \right] \tag{2.17}$$

The resultant forces and moments acting on the laminate are obtained by integration of the stresses in each layer or lamina through the laminate thickness, for example,

$$N_x = \int_{-t/2}^{-t/2} \sigma_x dz, M_x = \int_{-t/2}^{-t/2} \sigma_x z dz,$$

(2.18)

where, N_x and M_x are the force and moment per unit width of the cross section of the laminate (**Fig. 2.7**)

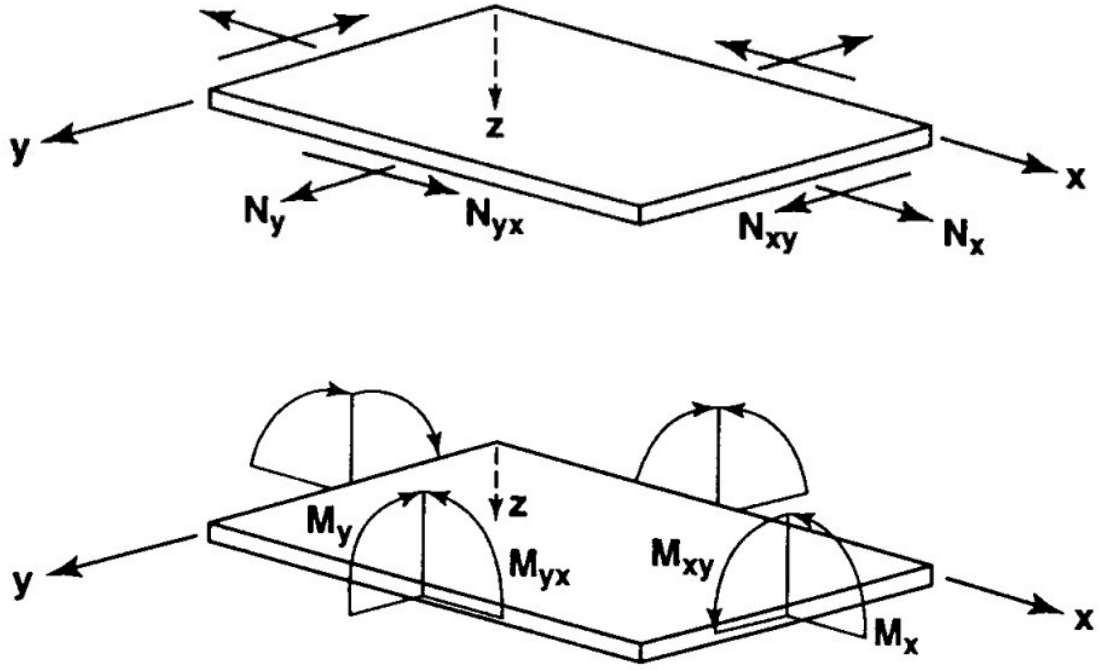

Fig 2.7. In-plane Forces & Moments on a Flat Laminate

N_x and M_x for the entire laminate is obtained upon integration over the entire laminate,

$$\begin{bmatrix} N_x \\ N_y \\ N_{xy} \end{bmatrix} = \int_{-t/2}^{t/2} \begin{bmatrix} \sigma_x \\ \sigma_y \\ \tau_{xy} \end{bmatrix} dz = \sum_{k=1}^{N} \int_{z_{k-1}}^{z_k} \begin{bmatrix} \sigma_x \\ \sigma_y \\ \tau_{xy} \end{bmatrix}_k dz$$

(2.19a)

$$\begin{bmatrix} M_x \\ M_y \\ M_{xy} \end{bmatrix} = \int_{-t/2}^{t/2} \begin{bmatrix} \sigma_x \\ \sigma_y \\ \tau_{xy} \end{bmatrix} z dz = \sum_{k=1}^{N} \int_{z_{k-1}}^{z_k} \begin{bmatrix} \sigma_x \\ \sigma_y \\ \tau_{xy} \end{bmatrix}_k z dz$$

(2.19b)

where z_k and z_{k-1} are defined in the basis laminate geometry in **Fig. 2.6**. These forces and moment resultants do not depend on z after integration, but are functions of x and y, the coordinates in the plane of the laminate middle surface.

Taking advantage of the fact that the stiffness matrix for a lamina is often constant within the lamina (unless the lamina has temperature dependent or moisture dependent properties and a temperature or moisture gradient exists across the lamina). If the elevated temperature and moisture are constant through the thickness of the lamina, then the values of $[\overline{Q_{ij}}]$ are constant in the layer. Thus, the stiffness matrix goes outside the integration over each layer, but is within the summation of force and moment resultants for each layer.

When the lamina stress-strain relations (Eq.2.15) are substituted, the forces and moments become

$$\begin{bmatrix} N_x \\ N_y \\ N_{xy} \end{bmatrix} = \sum_{k=1}^{N} \begin{bmatrix} \bar{Q}_{11} & \bar{Q}_{12} & \bar{Q}_{16} \\ \bar{Q}_{12} & \bar{Q}_{22} & \bar{Q}_{26} \\ \bar{Q}_{16} & \bar{Q}_{26} & \bar{Q}_{66} \end{bmatrix}_k \left[\int_{z_{k-1}}^{z_k} \begin{bmatrix} \varepsilon_x^0 \\ \varepsilon_y^0 \\ \gamma_{xy}^0 \end{bmatrix} dz + \int_{z_{k-1}}^{z_k} \begin{bmatrix} \kappa_x \\ \kappa_y \\ \kappa_{xy} \end{bmatrix} z dz \right]$$

$$\begin{bmatrix} M_x \\ M_y \\ M_{xy} \end{bmatrix} = \sum_{k=1}^{N} \begin{bmatrix} \bar{Q}_{11} & \bar{Q}_{12} & \bar{Q}_{16} \\ \bar{Q}_{12} & \bar{Q}_{22} & \bar{Q}_{26} \\ \bar{Q}_{16} & \bar{Q}_{26} & \bar{Q}_{66} \end{bmatrix}_k \left[\int_{z_{k-1}}^{z_k} \begin{bmatrix} \varepsilon_x^0 \\ \varepsilon_y^0 \\ \gamma_{xy}^0 \end{bmatrix} z dz + \int_{z_{k-1}}^{z_k} \begin{bmatrix} \kappa_x \\ \kappa_y \\ \kappa_{xy} \end{bmatrix} z^2 dz \right]$$

(2.20)

Recalling that $\varepsilon_x^0, \varepsilon_y^0, \varepsilon_z^0, \kappa_x, \kappa_y, \kappa_{xy}$ are not functions of z, but are middle surface values so they can be removed from the summation. Hence Eq. 2.14 can be written as

$$\begin{bmatrix} N_x \\ N_y \\ N_{xy} \end{bmatrix} = \begin{bmatrix} A_{11} & A_{12} & A_{16} \\ A_{12} & A_{22} & A_{26} \\ A_{16} & A_{26} & A_{66} \end{bmatrix} \begin{bmatrix} \varepsilon_x^0 \\ \varepsilon_y^0 \\ \gamma_{xy}^0 \end{bmatrix} + \begin{bmatrix} B_{11} & B_{12} & B_{16} \\ B_{12} & B_{22} & B_{26} \\ B_{16} & B_{26} & B_{66} \end{bmatrix} \begin{bmatrix} \kappa_x \\ \kappa_y \\ \kappa_{xy} \end{bmatrix}$$

$$\begin{bmatrix} M_x \\ M_y \\ M_{xy} \end{bmatrix} = \begin{bmatrix} B_{11} & B_{12} & B_{16} \\ B_{12} & B_{22} & B_{26} \\ B_{16} & B_{26} & B_{66} \end{bmatrix} \begin{bmatrix} \varepsilon_x^0 \\ \varepsilon_y^0 \\ \gamma_{xy}^0 \end{bmatrix} + \begin{bmatrix} D_{11} & D_{12} & D_{16} \\ D_{12} & D_{22} & D_{26} \\ D_{16} & D_{26} & D_{66} \end{bmatrix} \begin{bmatrix} \kappa_x \\ \kappa_y \\ \kappa_{xy} \end{bmatrix} \tag{2.21}$$

Where,

$$A_{ij} = \sum_{k=1}^{N} (\bar{Q}_{ij})_k (z_k - z_{k-1})$$

$$B_{ij} = \frac{1}{2} \sum_{k=1}^{N} (\bar{Q}_{ij})_k (z_k^2 - z_{k-1}^2)$$

$$D_{ij} = \frac{1}{3} \sum_{k=1}^{N} (\bar{Q}_{ij})_k (z_k^3 - z_{k-1}^3) \tag{2.22}$$

Combining the above relations (Eq. 2.16 and 2.17) and including the transverse shear resultants, the in-plane stress resultants {N}, the moments resultants{M}, and the transverse shear resultants {Q}, are related to the midplane strains and curvatures for a general laminated shell element as

$$\begin{Bmatrix} N_x \\ N_y \\ N_{xy} \\ M_x \\ M_y \\ M_{xy} \\ Q_y \\ Q_x \end{Bmatrix} = \begin{bmatrix} A_{11} & A_{12} & A_{16} & B_{11} & B_{12} & B_{16} & 0 & 0 \\ A_{12} & A_{22} & A_{26} & B_{12} & B_{22} & B_{26} & 0 & 0 \\ A_{16} & A_{26} & A_{66} & B_{16} & B_{26} & B_{66} & 0 & 0 \\ B_{11} & B_{12} & B_{16} & D_{11} & D_{12} & D_{16} & 0 & 0 \\ B_{12} & B_{22} & B_{26} & D_{12} & D_{22} & D_{26} & 0 & 0 \\ B_{16} & B_{26} & B_{66} & D_{16} & D_{26} & D_{66} & 0 & 0 \\ 0 & 0 & 0 & 0 & 0 & 0 & A_{44} & A_{45} \\ 0 & 0 & 0 & 0 & 0 & 0 & A_{45} & A_{55} \end{bmatrix} \begin{Bmatrix} \varepsilon_{xx}^0 \\ \varepsilon_{yy}^0 \\ \gamma_{xy}^0 \\ k_x \\ k_y \\ k_{xy} \\ \gamma_{yz} \\ \gamma_{xz} \end{Bmatrix} \tag{2.23a}$$

Where, N_x, N_y and N_{xy} are in-plane stress resultants, M_x, M_y and M_{xy} are moment resultants and Q_x, Q_y are transverse shear stress resultants.
In short,

$$\{N\} = [A]\{\varepsilon^0\} + [B]\{\kappa\}$$
$$\{M\} = [B]\{\varepsilon^0\} + [D]\{\kappa\}$$
$$\{Q\} = [A^*]\{\gamma\}$$

(2.23b)

where, $[A]$, $[B]$ and $[D]$ are the stiffness coefficients.

The extensional, bending-stretching and bending stiffnesses of the laminate are expressed in the usual form as

$$(A_{ij},\, B_{ij},\, D_{ij}) = \sum_{k=1}^{n} \int_{Z_{k-1}}^{Z_k} (\bar{Q}_{ij})_k (1, z, z^2)\, \mathrm{d}z, \quad i,j = 1,2,6.$$

(2.23c)

Similarly, the shear stiffness is expressed as

$$\left(A_{ij}^*\right) = \sum_{k=1}^{n} \int_{z_{k-1}}^{z_k} \alpha(\bar{Q}_{ij})_k dz, i, j = 4,5$$

(2.23d)

α, the shear correction factor which is derived from the Timoshenko beam concept by applying the energy principle and is assumed as 5/6. It accounts for the non-uniform distribution of transverse shear stress across the thickness of the laminate.

2.4 *FINITE ELEMENT FORMULATION*

The finite element formulations and the solution details are presented here. An eight noded isoparametric element is employed, both the geometry and displacement field of which are expressed in terms of the same shape functions. The parent element in local natural coordinate system can be mapped to an arbitrary shape in the Cartesian coordinate system.

2.4.1 *QUADRATIC ISOPARAMETRIC ELEMENT*

Consider an eight noded isoparametric element **Figs 2.8(a)** & **(b)** with five degrees of freedom at each node, viz. $u^0, v^0, w^0, \theta_x, \theta_y$. The element geometry and displacement field are expressed by the quadratic shape functions (N_i).

$$x = \sum_{i=1}^{8} N_i x_i \qquad y = \sum_{i=1}^{8} N_i y_i \tag{2.24}$$

Where x_i and y_i are the global coordinate at a node i.

By using the eight-noded element shape functions, the element displacements are expressed in terms of their nodal values given by

$$u^0 = \sum_{i=1}^{8} N_i u_i^0, \quad v^0 = \sum_{i=1}^{8} N_i v_i^0, \quad w = \sum_{i=1}^{8} N_i w_i, \quad \theta_x = \sum_{i=1}^{8} N_i \theta_{xi}, \quad \theta_y = \sum_{i=1}^{8} N_i \theta_{yi} \tag{2.25}$$

where N_i*'s* are the shape functions used to interpolate the generalized displacements, u_i^0, v_i^0, w_i , θ_{xi}, θ_{yi} at node *i* within an element.

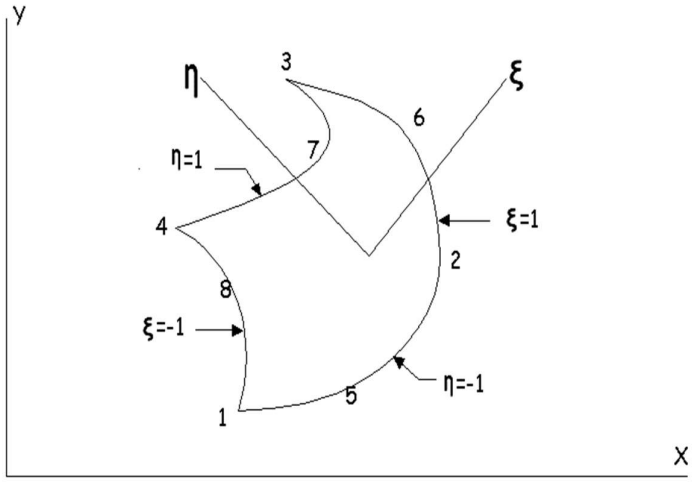

Fig 2.8(a). Mapping of the element in X-Y plane

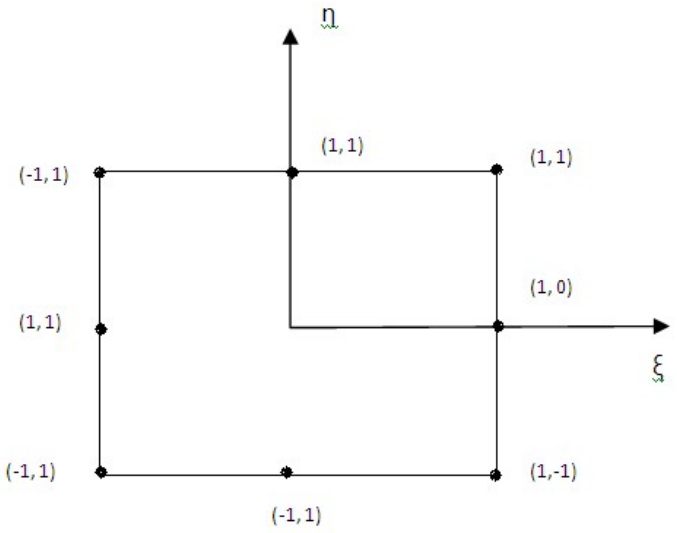

Fig 2.8(b). The element in the $\xi - \eta$ space

An eight noded isoparametric quadratic plate bending element with five degrees of freedom at each node (three translations and two rotations) is considered wherein the shape functions are given as [58]

$$N_i = (1 + \xi\xi_i)(1 + \eta\eta_i)(\xi\xi_i + \eta\eta_i - 1)/4 \cdots\cdots i = 1,2,3,4$$
$$N_i = (1 - \xi^2)(1 + \eta\eta_i)/2 \cdots\cdots i = 5,7$$
$$N_i = (1 - \eta^2)(1 + \xi\xi_i)/2 \cdots\cdots i = 6,8$$

(2.26)

Where, ξ and η are the local natural coordinates of the element and ξ_i and η_i are the values at a node "i", i ranges from 1 to 8.

$$\begin{bmatrix} N_{i,x} \\ \\ N_{i,y} \end{bmatrix} = [J]^{-1} \begin{bmatrix} N_{i,\xi} \\ \\ N_{i,\eta} \end{bmatrix}$$

$$[J] = \begin{bmatrix} x_{,\xi} & y_{,\xi} \\ x_{,n} & y_{,n} \end{bmatrix}$$

(2.27)

where, [J] is the Jacobian Matrix.

2.4.2 *ELEMENT STIFFNESS MATRIX*

The potential energy of deformation for the element, is expressed as

$$U_e = \frac{1}{2}\int\int_A \{\varepsilon\}^T [D] \{\varepsilon\} dA$$

(2.28)

If $\{\varepsilon\} = [B]\{\delta_e\} = [[B_1].....[B_8]] \{\delta_e\}$

Where $\{\delta_e\} = \{\overline{u_1} \quad \overline{v_1} \quad w_1 \quad \theta_{x1} \quad \theta_{y1} .....\overline{u_8} \quad \overline{v_8} \quad w_8 \quad \theta_{x8} \quad \theta_{y8}\}^T$

(2.29)

Then,

$$U_e = \frac{1}{2}\int_{-a/2}^{a/2}\int_{-b/2}^{b/2} \{\delta_e\}^T [B]^T [D][B]\{\delta_e\} dxdy$$

$$= \frac{1}{2}\{\delta_e\}^t [K_e]\{\delta_e\}$$

(2.30)

In which,

$$[K_e] = \int_{-a/2}^{a/2}\int_{-b/2}^{b/2} [B]^T [D][B] dxdy$$

(2.31)

$[B_i]$, the Strain-Displacement Matrix in the above equation is given by

$$[B_{ii}] = \begin{bmatrix} N_{i,x} & 0 & N_i/R_x & 0 & 0 \\ 0 & N_{i,y} & N_i/R_y & 0 & 0 \\ N_{i,y} & N_{i,x} & N_i/R_{xy} & 0 & 0 \\ 0 & 0 & 0 & 0 & N_{i,x} \\ 0 & 0 & 0 & -N_{i,y} & 0 \\ 0 & 0 & 0 & -N_{i,x} & N_{i,y} \\ 0 & 0 & N_{i,x} & 0 & N_i \\ 0 & 0 & N_{i,y} & -N_i & 0 \end{bmatrix}$$

(i = 1 to 8)

For twisted plates,

$$N_i/R_x = N_i/R_y = 0$$

For twisted conical shells,

$$N_i/R_x = 0$$

Now, $dxdy = |J|d\xi d\eta$, where $[J]$ is the determinant of the Jacobian matrix, the element stiffness matrix can be expressed in local natural coordinates of the element as

$$[K_e] = \int_{-1}^{1}\int_{-1}^{1} [B]^T [D] [B] |J| \, d\xi d\eta$$

(2.32)

Where, [B] is the strain-displacement matrix, [D], the elasticity matrix and J is the determinant of the Jacobian matrix. Reduced integration (2X2) is employed to avoid the shear locking.

2.4.3 *ELEMENT MASS MATRIX*

Similar to the case of stiffness matrix, the consistent element mass matrix $[M_e]$ is expressed as

$$[M_e] = \int_{-1}^{1}\int_{-1}^{1} [N]^T [\rho] [N] J \, d\xi \, d\eta$$

where [N] is the shape function matrix and [ρ] is the inertia matrix.

[N] Is given by

$$[N] = [[N_1] \ldots\ldots\ldots\ldots [N_8]] \tag{2.33}$$

where,

$$[N_i] = \begin{bmatrix} N_i & & & & \\ 0 & N_i & Symmetric & & \\ 0 & 0 & N_i & & \\ 0 & 0 & 0 & N_i & \\ 0 & 0 & 0 & 0 & N_i \end{bmatrix} \tag{2.34}$$

$[M_e]$ is calculated using (2 x 2) Gauss quadrature.

2.5 *DYNAMIC EQUILIBRIUM EQUATIONS*

The dynamic equilibrium equation for moderate rotational speeds is derived employing Lagrange's equation of motion and neglecting Coriolis effect the equation in global form is expressed as [59]

$$[M]\{\ddot{\delta}\} + ([K] + [K_\sigma])\{\delta\} = 0 \tag{2.35}$$

Where, [M], [K], [K_σ] are global mass, elastic stiffness and geometric stiffness matrices, respectively. $\{F(\Omega^2)\}$ is the nodal equivalent centrifugal forces and $\{\delta\}$ is the global displacement vector. [K_σ] depends on the initial stress distribution and is obtained by the iterative procedure [60] upon solving

$$([K] + [K_\sigma])\{\delta\} = 0 \tag{2.36}$$

The matrix of angular velocity components contributing towards acceleration vector is given as [59,61]

$$[A] = \begin{bmatrix} \Omega_y{}^2 + \Omega_z{}^2 & -\Omega_x\Omega_y & -\Omega_x\Omega_z \\ -\Omega_x\Omega_y & \Omega_x{}^2 + \Omega_z{}^2 & -\Omega_y\Omega_z \\ -\Omega_x\Omega_z & -\Omega_y\Omega_z & \Omega_x{}^2 + \Omega_y{}^2 \end{bmatrix}$$

(2.37)

The element geometric stiffness matrix due to rotation is given by

$$[K_{\sigma\varepsilon}] = \int_{vol} [G]^T [M_\sigma][G]\, d(vol)]$$

(2.38)

Where, the matrix $[G]$ consists of derivatives of shape functions and $[M_\sigma]$ is the matrix of initial in-plane stress resultants caused by rotation.

The natural frequencies are determined from the standard eigenvalue problem which is represented below and is solved by QR iteration algorithm.

$$[A]\{\delta\} = \lambda\{\delta\}$$

where $[A] = ([K] + [K_\sigma])^{-1}[M]$ and $\lambda = 1/\omega_n{}^2$

(2.39)

CHAPTER - III

RESULTS AND DISCUSSION

3.1 *VALIDATION OF THE PRESENT FEM WORK*

3.1.1 Validation of Non-dimensional fundamental frequency parameter

Finite element codes are developed based on the present analysis and the results obtained by running these codes are validated with those in the existing literature. A mesh size of (8x8) consisting of 64 elements and 225 nodes is considered for the analysis. Each node of the isoparametric element is considered as having five degrees of freedom (three translations and two rotations).

The results obtained from the present FEM formulations are initially validated against the published works of Zhao (2009) [63] and the deviation in the results is found to be well within 1%. The natural frequencies corresponding the first four modes of vibration of the plates with FGM constituents of Al/Al2O3, Al/ZrO2 and Ti-6Al-4Vare compared with the available results for a range of the FGM power-index values (k=0, 0.5, 1, 2, 5, 8 and 10) and the validation results are presented in in **Table 3.2**. The close agreement of the present FEM results with the benchmark values confirms the accuracy the codes developed and their suitability in carrying out further analyses on the free vibration behavior of FGM plates.

Table 3.1(a, b, c, d) *Validation of Non-dimensional fundamental frequency parameter* $\omega^* = \omega a^2/t\sqrt{\rho_c/E_c}$

a. Al/Al_2O_3 FG plates

		k						
Zhao (2009)	Mode	0	0.5	1	2	5	8	10
	1	5.6763	4.8209	4.3474	3.9474	3.7218	3.641	3.5923
	2	13.537	11.539	10.416	9.4435	8.8448	8.6264	8.5037
	3	13.537	11.539	10.416	9.4435	8.8448	8.6264	8.5037
	4	20.633	17.639	15.936	14.431	13.445	13.082	12.887
Current FEM data		k						
	Mode	0	0.5	1	2	5	8	10
	1	5.7697	5.0068	4.6412	4.3324	4.0449	3.8804	3.7924
	2	13.7740	11.7520	10.6089	9.6270	9.0081	8.7796	8.6516
	3	13.7740	11.7520	10.6089	9.6270	9.0081	8.7796	8.6516
	4	21.1405	18.1259	16.4311	14.9499	13.9106	13.4956	13.2753

b. $SUS304/Si_3N_4$ FG plates

		k						
Zhao (2009)	Mode	0	0.5	1	2	5	8	10
	1	5.6148	3.8947	3.4242	3.0813	2.8058	2.7129	2.6768
	2	13.513	9.3645	8.2298	7.3991	6.7284	6.5032	6.4161
	3	13.513	9.3645	8.2298	7.3991	6.7284	6.5032	6.4161
	4	20.74	14.365	12.62	11.338	10.299	9.9517	9.8178
Current FEM data		k						
	Mode	0	0.5	1	2	5	8	10
	1	5.6813	3.9503	3.4759	3.1288	2.8443	2.7473	2.7095
	2	13.5979	9.4308	8.2838	7.4467	6.7707	6.5430	6.4545
	3	13.5979	9.4308	8.2838	7.4467	6.7707	6.5430	6.4545
	4	20.9137	14.4988	12.7335	11.4389	10.3865	10.0332	9.8966

c. Ti–6Al–4V/Aluminum oxide FG plates

		k						
Zhao (2009)	Mode	0	0.5	1	2	5	8	10
	1	5.6147	4.6754	4.2255	3.8897	3.6546	3.5435	3.4892
	2	13.42	11.257	10.114	9.2916	8.748	8.4729	8.3417
	3	13.42	11.257	10.114	9.2916	8.748	8.4729	8.3417
	4	20.484	17.2867	15.459	14.179	13.372	12.939	12.738
Current FEM data		k						
	Mode	0	0.5	1	2	5	8	10
	1	5.7080	4.7865	4.3979	4.0830	3.7810	3.6343	3.5652
	2	13.6507	11.3400	10.2917	9.4571	8.7982	8.5159	8.3810
	3	13.6507	11.3400	10.2917	9.4571	8.7982	8.5159	8.3810
	4	20.9809	17.4732	15.8818	14.5895	13.5153	13.0561	12.8419

d. Al/ZrO_2 FG plates

		k						
Zhao (2009)	Mode	0	0.5	1	2	5	8	10
	1	5.6763	5.1105	4.8713	4.6977	4.5549	4.4741	4.4323
	2	13.537	12.207	11.633	11.199	10.828	10.632	10.533
	3	13.537	12.207	11.633	11.199	10.828	10.632	10.533
	4	20.633	18.63	17.748	17.063	16.462	16.157	16.008
Current FEM data		k						
	Mode	0	0.5	1	2	5	8	10
	1	5.7697	5.2319	5.0169	4.8530	4.6782	4.5756	4.5248
	2	13.7740	12.4252	11.8368	11.3974	11.0227	10.8200	10.7172
	3	13.7740	12.4252	11.8368	11.3974	11.0227	10.8200	10.7172
	4	21.1405	19.1063	18.2114	17.5207	16.9006	16.5767	16.4170

3.1.2 Validation of Porosity Type

The free vibration response in the present study is compared with the results of a previously published paper by Kim, J. et al. (2019)[64] on "Bending, free vibration, and buckling of modified couples stress-based functionally graded porous micro-plates". The dimensions of functionally graded porous plate in this paper are a = 20t, b = 20t, and t = 17.6 × 10−6m. The moduli and mass densities of two constituents are E_t= 14.4GP a, E_t = 1.44GP a, ρ_t = 12.2 × 103kg/m, and ρ_b = 1.22 × 103kg/m. A mesh size of (8x8) consisting of 64 isoparametric elements and 225 nodes is considered in the present FE method for validation with the existing literature. The graph below shows the results are obtained converges with the data published previously.

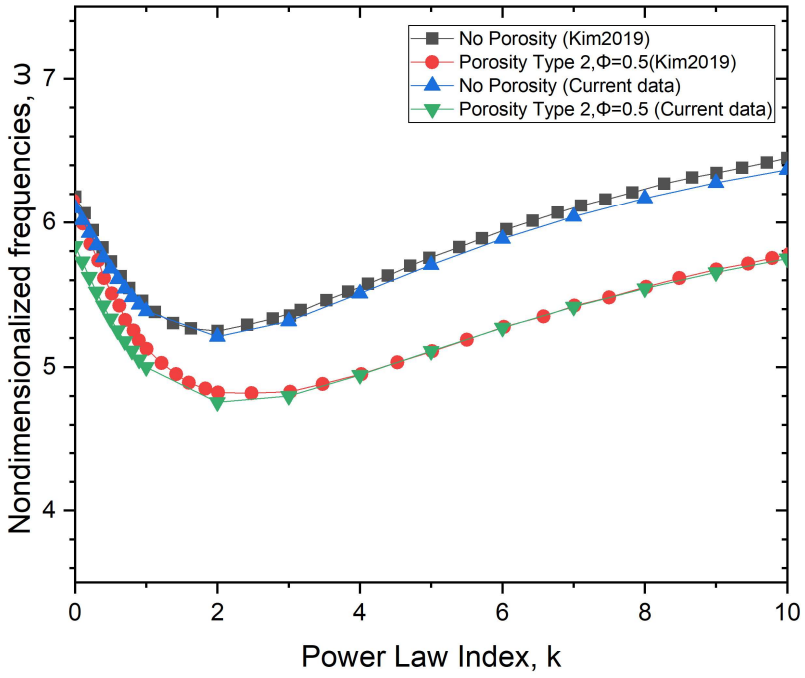

Fig 3.1. Variation of NDFF with power law index

3.1.3 Validation of Thermal Analysis

In order to check the accuracy of the present model, an FGM plate with a = b = 0.2 m and h = 0.025 m made from SUS304/Si_3N_4 with a constant Poisson's ratio of ν = 0.28 is considered. The frequency parameter $\omega^* = \omega a^2/t\sqrt{\rho_m(1-\nu^2)/E_m}$

computed by FE method is presented in Table 3.2 and are compared to the results presented by Huang et al.(2004) obtained by Reddy higher order shear deformation theory and Alijani et al.(2011) obtained by first order shear deformation theory. The frequency parameter is reported for different volume fraction exponents and different thermal variations.It is seen that the data obtained by present FE formulation are close to both the results published previously.

Table 3.2 *Validation of frequency parameter* $\omega^* = \omega a^2/t\sqrt{\rho_m(1-\nu^2)/E_m}$ *in thermal environment*

Temperature	k	Alijani(FSDT)	Huang2004	Current data
T_m = 300 K T_c = 300K	0	12.528	12.495	12.247
	0.5	8.622	8.675	8.523
	1	7.557	7.555	7.486
	2	6.786	6.777	6.729
T_m = 300 K T_c = 400 K	0	12.332	12.397	12.931
	0.5	8.468	8.615	8.81
	1	7.414	7.474	7.656
	2	6.649	6.693	6.823
T_m = 300 K T_c = 600 K	0	11.919	11.984	12.008
	0.5	8.138	8.269	8.247
	1	7.102	7.171	7.203
	2	6.346	6.398	6.452

PART A: FREE VIBRATION ANALYSIS

3.2 *MODEL ASSUMPTIONS*

For this study, a cantilevered square FGM plate with length(a)= breadth(b)=0.1m, and thickness(t)= 0.1*a, comprising of 4 different FGM constituent combinations are considered. The material properties are as given in the table below:

Table 3.3 *Properties of FGM components*

Material	*Properties*		
	E(N/m^2)	ν	ρ(kg/m^3)
Aluminium (Al)	70.0 X10^9	0.30	2707
Alumina (Al_2O_3)	380 X10^9	0.30	3800
Zirconia (ZrO_2)	151 X10^9	0.30	3000
Ti-6Al-4V	105.7 X10^9	0.298	4429
Aluminium Oxide	320.2 X10^9	0.26	3750
Stainless steel (SUS304)	207.78 X10^9	0.3177	8166
Silicon Nitride (Si_3N_4)	322.27 X10^9	0.24	2370

For these FGM combinations, free vibration characteristics for different volume fractions (k), aspect ratios (a/b), porosity types (0,1,2 & 3), twist angle(ψ) and rotational speed (ω) are demonstrated and discussed.

3.3 *RESULTS AND DISCUSSION OF FREE VIBRATION CHARACTERISTICS BY VARYING PARAMETERS*

3.3.1 Influence of varying Twist Angle(ψ) for different Porosity types

FGM 1: Al/Al_2O_3

Table 3.4(a) *The first and the second natural frequencies of square Al/Al_2O_3 FGM plates for different twist angles (ψ) and power index values (k) for no porosity (Type =0)*

		Porosity Type 0	
Twist Angle	**k**	**1st Freq.**	**2nd Freq.**
0˚	**0**	1.04E+00	2.44E+00
	0.5	8.85E-01	2.08E+00
	1	7.95E-01	1.87E+00
	2	7.20E-01	1.70E+00
	5	6.79E-01	1.59E+00
	10	6.52E-01	1.53E+00

		Porosity Type 0	
Twist Angle	**k**	**1st Freq.**	**2nd Freq.**
10˚	**0**	1.03E+00	2.52E+00
	0.5	8.79E-01	2.16E+00
	1	7.90E-01	1.94E+00
	2	7.15E-01	1.76E+00
	5	6.74E-01	1.64E+00
	10	6.48E-01	1.57E+00
20˚	**0**	1.01E+00	2.76E+00
	0.5	8.62E-01	2.39E+00
	1	7.74E-01	2.16E+00
	2	7.01E-01	1.96E+00
	5	6.61E-01	1.80E+00
	10	6.35E-01	1.71E+00
30˚	**0**	9.75E-01	3.18E+00
	0.5	8.30E-01	2.78E+00
	1	7.46E-01	2.53E+00
	2	6.76E-01	2.29E+00
	5	6.37E-01	2.07E+00
	10	6.12E-01	1.94E+00

Table 3.4(b) *The first and the second natural frequencies of square Al/Al_2O_3 FGM plates for different twist angles (ψ) and power index values (k) for Porosity Type 1*

		Porosity Type 1	
Twist Angle	**k**	**1st Freq.**	**2nd Freq.**
0˚	**0**	1.12E+00	2.68E+00
	0.5	9.46E-01	2.27E+00
	1	8.43E-01	2.03E+00
	2	7.64E-01	1.84E+00
	5	7.27E-01	1.74E+00
	10	7.05E-01	1.68E+00
10˚	**0**	1.12E+00	2.76E+00
	0.5	9.40E-01	2.34E+00
	1	8.37E-01	2.09E+00
	2	7.59E-01	1.90E+00
	5	7.23E-01	1.79E+00
	10	7.01E-01	1.72E+00
20˚	**0**	1.09E+00	2.98E+00
	0.5	9.22E-01	2.55E+00
	1	8.21E-01	2.30E+00
	2	7.44E-01	2.08E+00
	5	7.09E-01	1.94E+00
	10	6.87E-01	1.85E+00

		Porosity Type 1	
Twist Angle	**k**	**1st Freq.**	**2nd Freq.**
30˚	**0**	1.05E+00	3.37E+00
	0.5	8.88E-01	2.91E+00
	1	7.91E-01	2.64E+00
	2	7.17E-01	2.40E+00
	5	6.83E-01	2.21E+00
	10	6.61E-01	2.08E+00

Table 3.4(c) *The first and the second natural frequencies of square Al/Al_2O_3 FGM plates for different twist angles (ψ) and power index values (k) for Porosity Type 2*

		Porosity Type 2	
Twist Angle	**k**	**1st Freq.**	**2nd Freq.**
0˚	**0**	1.02E+00	2.48E+00
	0.5	8.59E-01	2.10E+00
	1	7.67E-01	1.88E+00
	2	6.88E-01	1.69E+00
	5	6.45E-01	1.58E+00
	10	6.27E-01	1.53E+00
10˚	**0**	1.01E+00	2.56E+00
	0.5	8.53E-01	2.18E+00
	1	7.62E-01	1.96E+00
	2	6.84E-01	1.76E+00
	5	6.41E-01	1.64E+00
	10	6.23E-01	1.58E+00
20˚	**0**	9.93E-01	2.80E+00
	0.5	8.37E-01	2.41E+00
	1	7.47E-01	2.18E+00
	2	6.71E-01	1.97E+00
	5	6.29E-01	1.81E+00
	10	6.11E-01	1.72E+00
30˚	**0**	9.56E-01	3.22E+00
	0.5	8.06E-01	2.81E+00
	1	7.20E-01	2.57E+00
	2	6.47E-01	2.33E+00
	5	6.06E-01	2.10E+00
	10	5.89E-01	1.98E+00

Table 3.4(d) *The first and the second natural frequencies of square Al/Al_2O_3 FGM plates for different twist angles (ψ) and power index values (k) for Porosity Type 3*

		Porosity Type 3	
Twist Angle	**k**	**1st Freq.**	**2nd Freq.**
0˚	**0**	1.02E+00	2.48E+00
	0.5	8.78E-01	2.14E+00
	1	7.93E-01	1.93E+00
	2	7.25E-01	1.76E+00
	5	6.86E-01	1.66E+00
	10	6.50E-01	1.57E+00
10˚	**0**	1.01E+00	2.56E+00
	0.5	8.72E-01	2.21E+00
	1	7.88E-01	2.00E+00
	2	7.21E-01	1.82E+00
	5	6.81E-01	1.70E+00
	10	6.46E-01	1.61E+00
20˚	**0**	9.93E-01	2.80E+00
	0.5	8.55E-01	2.43E+00
	1	7.72E-01	2.20E+00
	2	7.07E-01	1.99E+00
	5	6.68E-01	1.84E+00
	10	6.33E-01	1.74E+00
30˚	**0**	9.56E-01	3.22E+00
	0.5	8.24E-01	2.79E+00
	1	7.44E-01	2.54E+00
	2	7.44E-01	2.54E+00
	5	6.43E-01	2.08E+00
	10	6.10E-01	1.95E+00

The first and the second natural frequencies of square ***Al/Al_2O_3*** FGM plates for different combinations of twist angles (ψ) and power index values (k) are given in **Table 3.4(a)**, **Table 3.4(b)**, **Table 3.4(c)** and **Table 3.4(d)** for porosity types 0,1,2 and 3 respectively. The twist angle values are varied from 0˚ to 30˚ at a step of 10 degrees while the power index values are varied from 1 to 10. In general, the first natural frequencies are always found to be lower than the second natural frequency values. For a certain value of the power index k, the maximum value of the first natural frequencies is observed for the untwisted plate (ψ =0˚) and decreases with an increase in the twist angle (ψ). For example, at k=10, the fundamental frequencies are 6.52E-01, 6.48E-01, 6.35E-01 and 6.12E-01 for twist angles from 0˚, 10˚, 20˚ and 30˚ respectively (**Table 3.4(a)**). This clear trend of decrease in the natural frequency values is due to the fact that the stiffness of the plate decreases with an increase in the twist angle. However, the reverse trend is observed in case of the second natural frequencies wherein the values are found

to increase with an increase in the twist angle (ψ). Since the first natural frequency corresponds to the bending mode while the second natural frequency represents the torsional mode. The findings suggest that increase in the twist angle suppresses the bending mode and enhances the twisting mode in the twisted plate. For example, at k=5, the second natural frequencies are 1.59E+00, 1.64E+00, 1.80E+00 and 1.94E+00 for twist angles of 0˚, 10˚, 20˚ and 30˚ respectively(**Table 3.4(a)**). In case of both twisted and untwisted plates, both the first and second natural frequencies are found to decrease with an increase in the power index value for the range of the values considered (k=1 to 10). As evident, the contribution of the metallic constituents predominates with an increase in the power index value (k). As in this case the ceramic constituent Al_2O_3 with E=380 GPa has high strength compared to the metallic part Aluminium (Al) which is extremely soft with E=70 GPa. Thus an increase in the power index results in a decrease in the natural frequency values owing to the weakness due to transition towards the metallic properties. From **Table 3.(a)**, **Table 3.4(b)**, **Table 3.4(c)** and **Table 3.4(d)** it can be inferred that the highest values of both the first and second natural frequencies is observed for porosity type 1 while the lowest value is observed for porosity type 2.

FGM 2: $SUS304/Si_3N_4$

Table 3.5(a) *The first and the second natural frequencies of square SUS304/Si_3N_4 FGM plates for different twist angles (ψ) and power index values (k) for no porosity (Type 0)*

		Porosity Type 0	
Twist Angle	**k**	**1st Freq.**	**2nd Freq.**
0˚	**0**	1.03E+00	2.48E+00
	0.5	7.13E-01	1.70E+00
	1	6.25E-01	1.48E+00
	2	5.61E-01	1.32E+00
	5	5.10E-01	1.20E+00
	10	4.85E-01	1.14E+00
10˚	**0**	1.02E+00	2.55E+00
	0.5	7.08E-01	1.75E+00
	1	6.21E-01	1.53E+00
	2	5.58E-01	1.37E+00
	5	5.07E-01	1.24E+00
	10	4.82E-01	1.17E+00

		Porosity Type 0	
Twist Angle	**k**	**1st Freq.**	**2nd Freq.**
20˚	**0**	1.00E+00	2.79E+00
	0.5	6.94E-01	1.92E+00
	1	6.08E-01	1.68E+00
	2	5.47E-01	1.50E+00
	5	4.97E-01	1.35E+00
	10	4.73E-01	1.28E+00
30˚	**0**	9.64E-01	3.21E+00
	0.5	6.69E-01	2.22E+00
	1	5.86E-01	1.93E+00
	2	5.27E-01	1.72E+00
	5	4.79E-01	1.55E+00
	10	4.55E-01	1.47E+00

Table 3.5(b) *The first and the second natural frequencies of square SUS304/Si_3N_4 FGM plates for different twist angles (ψ) and power index values (k) for Porosity Type 1*

		Porosity Type 1	
Twist Angle	**k**	**1st Freq.**	**2nd Freq.**
0˚	**0**	1.11E+00	2.72E+00
	0.5	7.66E-01	1.85E+00
	1	6.75E-01	1.62E+00
	2	6.12E-01	1.47E+00
	5	5.60E-01	1.34E+00
	10	5.31E-01	1.27E+00
10˚	**0**	1.11E+00	2.79E+00
	0.5	7.61E-01	1.90E+00
	1	6.71E-01	1.67E+00
	2	6.08E-01	1.51E+00
	5	5.56E-01	1.37E+00
	10	5.28E-01	1.30E+00
20˚	**0**	1.09E+00	3.01E+00
	0.5	7.46E-01	2.06E+00
	1	6.58E-01	1.81E+00
	2	5.96E-01	1.63E+00
	5	5.45E-01	1.48E+00
	10	5.17E-01	1.40E+00
30˚	**0**	1.05E+00	3.40E+00
	0.5	7.19E-01	2.33E+00
	1	6.33E-01	2.04E+00
	2	5.74E-01	1.84E+00
	5	5.25E-01	1.67E+00
	10	4.98E-01	1.58E+00

Table 3.5(c) *The first and the second natural frequencies of square SUS304/Si_3N_4 FGM plates for different twist angles (ψ) and power index values (k) for Porosity Type 2*

		Porosity Type 2	
Twist Angle	**k**	**1st Freq.**	**2nd Freq.**
0˚	**0**	1.01E+00	2.51E+00
	0.5	7.23E-01	1.78E+00
	1	6.33E-01	1.56E+00
	2	5.66E-01	1.39E+00
	5	5.09E-01	1.25E+00
	10	4.81E-01	1.17E+00
10˚	**0**	1.01E+00	2.59E+00
	0.5	7.19E-01	1.84E+00
	1	6.29E-01	1.61E+00
	2	5.62E-01	1.43E+00
	5	5.06E-01	1.28E+00
	10	4.78E-01	1.21E+00
20˚	**0**	9.87E-01	2.83E+00
	0.5	7.04E-01	2.02E+00
	1	6.17E-01	1.77E+00
	2	5.51E-01	1.57E+00
	5	4.96E-01	1.40E+00
	10	4.69E-01	1.32E+00
30˚	**0**	9.51E-01	3.24E+00
	0.5	6.79E-01	2.32E+00
	1	5.95E-01	2.03E+00
	2	5.31E-01	1.81E+00
	5	4.78E-01	1.61E+00
	10	4.52E-01	1.51E+00

Table 3.5(d) *The first and the second natural frequencies of square SUS304/Si_3N_4 FGM plates for different twist angles (ψ) and power index values (k) for Porosity Type 3*

		Porosity Type 3	
Twist Angle	**k**	**1st Freq.**	**2nd Freq.**
0˚	**0**	1.01E+00	2.51E+00
	0.5	6.80E-01	1.67E+00
	1	5.97E-01	1.46E+00
	2	5.40E-01	1.31E+00
	5	4.95E-01	1.20E+00
	10	4.73E-01	1.15E+00

		Porosity Type 3	
Twist Angle	**k**	**1st Freq.**	**2nd Freq.**
10˚	**0**	1.01E+00	2.59E+00
	0.5	6.76E-01	1.72E+00
	1	5.93E-01	1.50E+00
	2	5.36E-01	1.35E+00
	5	4.92E-01	1.24E+00
	10	4.70E-01	1.18E+00
20˚	**0**	9.87E-01	2.83E+00
	0.5	6.63E-01	1.88E+00
	1	5.81E-01	1.64E+00
	2	5.26E-01	1.48E+00
	5	4.82E-01	1.35E+00
	10	4.60E-01	1.29E+00
30˚	**0**	9.51E-01	3.24E+00
	0.5	6.39E-01	2.16E+00
	1	5.60E-01	1.88E+00
	2	5.06E-01	1.69E+00
	5	4.64E-01	1.54E+00
	10	4.44E-01	1.47E+00

The first and the second natural frequencies of square $\boldsymbol{SUS304/Si_3N_4}$ FGM plates for different combinations of twist angles (ψ) and power index values (k) are given in **Table 3.5(a)**, **Table 3.5(b)**, **Table 3.5(c)** and **Table 3.5(d)** for porosity types 0,1,2 and 3 respectively. The twist angle values are varied from 0˚ to 30˚ at a step of 10 degrees while the power index values are varied from 1 to 10. In general, the first natural frequencies are always found to be lower than the second natural frequency values. For a certain value of the power index k, the maximum value of the first natural frequencies is observed for the untwisted plate (ψ =0˚) and decreases with an increase in the twist angle (ψ). For example, at k=2, the fundamental frequencies are 5.61E-01, 5.58E-01, 5.47E-01 and 5.27E-01 for twist angles from 0˚, 10˚, 20˚ and 30˚ respectively for the plate with no porosity (**Table 3.5(a)**). This clear trend of decrease in the natural frequency values is due to the fact that the stiffness of the plate decreases with an increase in the twist angle. However, the reverse trend is observed in case of the second natural frequencies wherein the values are found to increase with an increase in the twist angle (ψ). Since the first natural frequency corresponds to the bending mode while the second natural frequency represents the torsional mode, the findings suggest that increase in the twist angle suppresses the bending mode and enhances the twisting mode in the twisted plate. For example, for the plate with porosity type 1 at k=0.5, the second natural frequencies are 1.85E+00, 1.90E+00,

2.06E+00 and 2.33E+00 (**Table 3.5(b)**) for twist angles of 0˚, 10˚, 20˚ and 30˚ respectively. In case of both twisted and untwisted plates, both the first and second natural frequencies are found to decrease with an increase in the power index value for the range of the values considered (k=1 to 10). As evident, the contribution of the metallic constituents predominates with an increase in the power index value (k). As in this case the ceramic constituent silicon nitride (Si_3N_4) with E=322.27 GPa has high strength compared to the metallic part stainless steel (SUS304) which is softer with E=207.78 GPa. Thus, an increase in the power index results in a decrease in the natural frequency values owing to the weakness due to transition towards the metallic properties. From **Table 3.5(a)**, **Table 3.5(b)**, **Table 3.5(c)** and **Table 3.5(d)** it can be inferred that the highest values of both the first and second natural frequencies for ***SUS304/Si_3N_4*** FGM plate is observed for porosity type 1 while the lowest value is observed for porosity type 3.

FGM 3: *Ti-6Al-4V/Aluminium Oxide*

Table 3.6(a) *The first and the second natural frequencies of square Ti-6Al-4V/Aluminium Oxide FGM plates for different twist angles (ψ) and power index values (k) for no porosity(Type 0)*

		Porosity Type 0	
Twist Angle	**k**	**1st Freq.**	**2nd Freq.**
0˚	**0**	1.03E+00	2.46E+00
	0.5	8.55E-01	2.04E+00
	1	7.74E-01	1.84E+00
	2	7.11E-01	1.68E+00
	5	6.64E-01	1.57E+00
	10	6.31E-01	1.49E+00
10˚	**0**	1.02E+00	2.54E+00
	0.5	8.50E-01	2.11E+00
	1	7.69E-01	1.90E+00
	2	7.07E-01	1.74E+00
	5	6.60E-01	1.61E+00
	10	6.27E-01	1.53E+00
20˚	**0**	1.00E+00	2.78E+00
	0.5	8.33E-01	2.32E+00
	1	7.54E-01	2.10E+00
	2	6.93E-01	1.91E+00
	5	6.47E-01	1.76E+00
	10	6.15E-01	1.66E+00
30˚	**0**	9.67E-01	3.20E+00
	0.5	8.03E-01	2.69E+00
	1	7.26E-01	2.43E+00
	2	6.68E-01	2.21E+00
	5	6.23E-01	2.01E+00
	10	5.92E-01	1.90E+00

Table 3.6(b) *The first and the second natural frequencies of square Ti-6Al-4V/Aluminium Oxide FGM plates for different twist angles (ψ) and power index values (k) for Porosity Type 1*

		Porosity Type 1	
Twist Angle	**k**	**1st Freq.**	**2nd Freq.**
0˚	**0**	1.12E+00	2.71E+00
	0.5	9.19E-01	2.22E+00
	1	8.30E-01	2.00E+00
	2	7.67E-01	1.85E+00
	5	7.22E-01	1.73E+00
	10	6.89E-01	1.65E+00
10˚	**0**	1.11E+00	2.78E+00
	0.5	9.13E-01	2.28E+00
	1	8.25E-01	2.06E+00
	2	7.62E-01	1.90E+00
	5	7.18E-01	1.77E+00
	10	6.85E-01	1.69E+00
20˚	**0**	1.09E+00	3.00E+00
	0.5	8.95E-01	2.48E+00
	1	8.09E-01	2.24E+00
	2	7.47E-01	2.06E+00
	5	7.03E-01	1.91E+00
	10	6.71E-01	1.81E+00
30˚	**0**	1.05E+00	3.39E+00
	0.5	8.62E-01	2.82E+00
	1	7.79E-01	2.56E+00
	2	7.20E-01	2.35E+00
	5	6.77E-01	2.16E+00
	10	6.46E-01	2.04E+00

Table 3.6(c) *The first and the second natural frequencies of square Ti-6Al-4V/Aluminium Oxide FGM plates for different twist angles (ψ) and power index values (k) for Porosity Type 2*

		Porosity Type 2	
Twist Angle	**k**	**1st Freq.**	**2nd Freq.**
0˚	**0**	1.02E+00	2.50E+00
	0.5	8.42E-01	2.07E+00
	1	7.60E-01	1.87E+00
	2	6.94E-01	1.71E+00
	5	6.47E-01	1.59E+00
	10	6.19E-01	1.51E+00
10˚	**0**	1.01E+00	2.58E+00
	0.5	8.36E-01	2.15E+00
	1	7.55E-01	1.94E+00
	2	6.90E-01	1.77E+00
	5	6.43E-01	1.64E+00
	10	6.15E-01	1.56E+00

		Porosity Type 2	
Twist Angle	**k**	**1st Freq.**	**2nd Freq.**
20˚	**0**	9.89E-01	2.82E+00
	0.5	8.20E-01	2.37E+00
	1	7.40E-01	2.15E+00
	2	6.76E-01	1.96E+00
	5	6.31E-01	1.79E+00
	10	6.03E-01	1.70E+00
30˚	**0**	9.53E-01	3.23E+00
	0.5	7.90E-01	2.74E+00
	1	7.13E-01	2.50E+00
	2	6.52E-01	2.27E+00
	5	6.07E-01	2.06E+00
	10	5.81E-01	1.94E+00

Table 3.6(d) *The first and the second natural frequencies of square Ti-6Al-4V/Aluminium Oxide FGM plates for different twist angles (ψ) and power index values (k) for Porosity Type 3*

		Porosity Type 3	
Twist Angle	**k**	**1st Freq.**	**2nd Freq.**
0˚	**0**	1.02E+00	2.50E+00
	0.5	8.41E-01	2.06E+00
	1	7.62E-01	1.87E+00
	2	7.05E-01	1.72E+00
	5	6.58E-01	1.60E+00
	10	6.21E-01	1.51E+00
10˚	**0**	1.01E+00	2.58E+00
	0.5	8.36E-01	2.13E+00
	1	7.58E-01	1.93E+00
	2	7.00E-01	1.77E+00
	5	6.53E-01	1.64E+00
	10	6.17E-01	1.55E+00
20˚	**0**	9.89E-01	2.82E+00
	0.5	8.19E-01	2.33E+00
	1	7.43E-01	2.11E+00
	2	6.86E-01	1.93E+00
	5	6.41E-01	1.78E+00
	10	6.05E-01	1.68E+00
30˚	**0**	9.53E-01	3.23E+00
	0.5	7.89E-01	2.68E+00
	1	7.16E-01	2.42E+00
	2	6.61E-01	2.20E+00
	5	6.17E-01	2.01E+00
	10	5.83E-01	1.90E+00

FGM 4: Al/ZrO_2

Table 3.7(a) *The first and the second natural frequencies of square Al/ZrO_2 FGM plates for different twist angles (ψ) and power index values (k) for no porosity(Type 0)*

		Porosity Type 0	
Twist Angle	**k**	**1st Freq.**	**2nd Freq.**
0˚	**0**	1.04E+00	2.44E+00
	0.5	9.36E-01	2.20E+00
	1	8.91E-01	2.09E+00
	2	8.59E-01	2.02E+00
	5	8.32E-01	1.95E+00
	10	8.08E-01	1.89E+00
10˚	**0**	1.03E+00	2.52E+00
	0.5	9.30E-01	2.28E+00
	1	8.85E-01	2.17E+00
	2	8.53E-01	2.08E+00
	5	8.27E-01	2.01E+00
	10	8.02E-01	1.95E+00
20˚	**0**	1.01E+00	2.76E+00
	0.5	9.12E-01	2.51E+00
	1	8.68E-01	2.38E+00
	2	8.36E-01	2.29E+00
	5	8.11E-01	2.20E+00
	10	7.87E-01	2.13E+00
30˚	**0**	9.75E-01	3.18E+00
	0.5	8.79E-01	2.90E+00
	1	8.36E-01	2.76E+00
	2	8.06E-01	2.63E+00
	5	7.81E-01	2.51E+00
	10	7.58E-01	2.43E+00

Table 3.7(b) *The first and the second natural frequencies of square Al/ZrO_2 FGM plates for different twist angles (ψ) and power index values (k) for Porosity type 1*

		Porosity Type 1	
Twist Angle	**k**	**1st Freq.**	**2nd Freq.**
0˚	**0**	1.12E+00	2.68E+00
	0.5	1.01E+00	2.41E+00
	1	9.59E-01	2.29E+00
	2	9.27E-01	2.21E+00
	5	9.02E-01	2.15E+00
	10	8.77E-01	2.09E+00

		Porosity Type 1	
Twist Angle	**k**	**1st Freq.**	**2nd Freq.**
10˚	**0**	1.12E+00	2.76E+00
	0.5	1.00E+00	2.48E+00
	1	9.53E-01	2.36E+00
	2	9.21E-01	2.28E+00
	5	8.96E-01	2.21E+00
	10	8.72E-01	2.14E+00
20˚	**0**	1.09E+00	2.98E+00
	0.5	9.82E-01	2.69E+00
	1	9.34E-01	2.56E+00
	2	9.03E-01	2.46E+00
	5	8.79E-01	2.38E+00
	10	8.55E-01	2.31E+00
30˚	**0**	1.05E+00	3.37E+00
	0.5	9.46E-01	3.06E+00
	1	9.00E-01	2.91E+00
	2	8.69E-01	2.79E+00
	5	8.46E-01	2.68E+00
	10	8.23E-01	2.60E+00

Table 3.7(c) *The first and the second natural frequencies of square Al/ZrO_2 FGM plates for different twist angles (ψ) and power index values (k) for Porosity type 2*

		Porosity Type 2	
Twist Angle	**k**	**1st Freq.**	**2nd Freq.**
0˚	**0**	1.02E+00	2.48E+00
	0.5	9.14E-01	2.23E+00
	1	8.67E-01	2.12E+00
	2	8.33E-01	2.03E+00
	5	8.09E-01	1.97E+00
	10	7.90E-01	1.92E+00
10˚	**0**	1.01E+00	2.56E+00
	0.5	9.08E-01	2.31E+00
	1	8.61E-01	2.19E+00
	2	8.28E-01	2.10E+00
	5	8.04E-01	2.04E+00
	10	7.85E-01	1.98E+00
20˚	**0**	9.93E-01	2.80E+00
	0.5	8.90E-01	2.54E+00
	1	8.44E-01	2.42E+00
	2	8.11E-01	2.31E+00
	5	7.89E-01	2.22E+00
	10	7.70E-01	2.16E+00

		Porosity Type 2	
Twist Angle	k	1st Freq.	2nd Freq.
30˚	0	9.56E-01	3.22E+00
	0.5	8.58E-01	2.94E+00
	1	8.14E-01	2.80E+00
	2	7.82E-01	2.67E+00
	5	7.60E-01	2.55E+00
	10	7.42E-01	2.47E+00

Table 3.7(d) *The first and the second natural frequencies of square Al/ZrO_2 FGM plates for different twist angles (ψ) and power index values (k) for Porosity type 3*

		Porosity Type 3	
Twist Angle	k	1st Freq.	2nd Freq.
0˚	0	1.02E+00	2.48E+00
	0.5	9.24E-01	2.25E+00
	1	8.82E-01	2.15E+00
	2	8.52E-01	2.07E+00
	5	8.23E-01	2.00E+00
	10	7.94E-01	1.93E+00
10˚	0	1.01E+00	2.56E+00
	0.5	9.18E-01	2.32E+00
	1	8.77E-01	2.22E+00
	2	8.47E-01	2.13E+00
	5	8.18E-01	2.06E+00
	10	7.89E-01	1.99E+00
20˚	0	9.93E-01	2.80E+00
	0.5	9.00E-01	2.54E+00
	1	8.59E-01	2.42E+00
	2	8.30E-01	2.32E+00
	5	8.01E-01	2.23E+00
	10	7.74E-01	2.16E+00
30˚	0	9.56E-01	3.22E+00
	0.5	8.67E-01	2.92E+00
	1	8.28E-01	2.77E+00
	2	8.00E-01	2.65E+00
	5	7.72E-01	2.53E+00
	10	7.45E-01	2.45E+00

The same trend of decreasing first natural frequency and increasing second natural frequency with increasing twist angle is seen in ***Ti-6Al-4V/Aluminium Oxide*** and ***Al/ZrO_2*** FG plates as previously seen in FGM 1 and FGM 2, irrespective of porosity type. Also, both the first and second natural frequencies

are found to decrease with an increase in the power index value for the range of the values considered (k=1 to 10), for both twisted and untwisted plates.

However, from **Table 3.5** and **Table 3.6** it can be inferred that the highest values of both the first and second natural frequencies for both ***Ti-6Al-4V/Aluminium Oxide*** and ***Al/ZrO_2*** FGM plates are observed for porosity type 1 while the lowest value is observed for porosity type 2.

3.3.2 Influence of varying Aspect Ratio (*a/b*) for different Porosity Types

FGM 1: Al/Al_2O_3

Table 3.8(a) *The first and the second natural frequencies of untwisted(ψ=0) Al/Al_2O_3 FGM plates for different aspect ratios(a/b) and power index values (k) for no porosity(Type 0)*

		Porosity Type 0	
Aspect Ratio	**k**	**1st Freq.**	**2nd Freq.**
1	**0**	1.04E+00	2.44E+00
	0.5	8.85E-01	2.08E+00
	1	7.95E-01	1.87E+00
	2	7.20E-01	1.70E+00
	5	6.79E-01	1.59E+00
	10	6.52E-01	1.53E+00
2	**0**	1.03E+00	4.02E+00
	0.5	8.75E-01	3.42E+00
	1	7.86E-01	3.07E+00
	2	7.12E-01	2.76E+00
	5	6.71E-01	2.56E+00
	10	6.45E-01	2.44E+00
5	**0**	1.01E+00	1.97E+00
	0.5	8.63E-01	1.77E+00
	1	7.76E-01	1.64E+00
	2	7.03E-01	1.48E+00
	5	6.63E-01	1.28E+00
	10	6.37E-01	1.16E+00
10	**0**	1.01E+00	1.01E+00
	0.5	8.60E-01	9.05E-01
	1	7.72E-01	8.38E-01
	2	7.00E-01	7.56E-01
	5	6.52E-01	6.60E-01
	10	5.93E-01	6.34E-01

Table 3.8(b) *The first and the second natural frequencies of untwisted(ψ=0) Al/Al_2O_3 FGM plates for different aspect ratios(a/b) and power index values (k) for Porosity type 1*

		Porosity Type 1	
Aspect Ratio	**k**	**1st Freq.**	**2nd Freq.**
1	**0**	1.12E+00	2.68E+00
	0.5	9.46E-01	2.27E+00
	1	8.43E-01	2.03E+00
	2	7.64E-01	1.84E+00
	5	7.27E-01	1.74E+00
	10	7.05E-01	1.68E+00
2	**0**	1.11E+00	4.37E+00
	0.5	9.39E-01	3.70E+00
	1	8.36E-01	3.29E+00
	2	7.58E-01	2.96E+00
	5	7.22E-01	2.74E+00
	10	6.99E-01	2.59E+00
5	**0**	1.10E+00	1.98E+00
	0.5	9.31E-01	1.77E+00
	1	8.30E-01	1.64E+00
	2	7.52E-01	1.50E+00
	5	7.16E-01	1.32E+00
	10	6.93E-01	1.20E+00
10	**0**	1.01E+00	1.10E+00
	0.5	9.03E-01	9.29E-01
	1	8.28E-01	8.39E-01
	2	7.50E-01	7.66E-01
	5	6.72E-01	7.14E-01
	10	6.12E-01	6.92E-01

Table 3.8(c) *The first and the second natural frequencies of untwisted(ψ=0) Al/Al_2O_3 FGM plates for different aspect ratios(a/b) and power index values (k) for Porosity type 2*

		Porosity Type 2	
Aspect Ratio	**k**	**1st Freq.**	**2nd Freq.**
1	**0**	1.02E+00	2.48E+00
	0.5	8.59E-01	2.10E+00
	1	7.67E-01	1.88E+00
	2	6.88E-01	1.69E+00
	5	6.45E-01	1.58E+00
	10	6.27E-01	1.53E+00
2	**0**	1.01E+00	4.11E+00
	0.5	8.54E-01	3.46E+00
	1	7.63E-01	3.10E+00
	2	6.85E-01	2.77E+00
	5	6.42E-01	2.56E+00
	10	6.24E-01	2.46E+00

		Porosity Type 2	
Aspect Ratio	**k**	**1st Freq.**	**2nd Freq.**
5	**0**	1.01E+00	1.97E+00
	0.5	8.49E-01	1.80E+00
	1	7.58E-01	1.69E+00
	2	6.81E-01	1.54E+00
	5	6.38E-01	1.34E+00
	10	6.20E-01	1.21E+00
10	**0**	1.00E+00	1.01E+00
	0.5	8.47E-01	9.22E-01
	1	7.57E-01	8.64E-01
	2	6.79E-01	7.90E-01
	5	6.37E-01	6.86E-01
	10	6.18E-01	6.19E-01

Table 3.8(d) *The first and the second natural frequencies of untwisted(ψ=0) Al/Al_2O_3 FGM plates for different aspect ratios(a/b) and power index values (k) for Porosity type 3*

		Porosity Type 3	
Aspect Ratio	**k**	**1st Freq.**	**2nd Freq.**
1	**0**	1.02E+00	2.48E+00
	0.5	8.78E-01	2.14E+00
	1	7.93E-01	1.93E+00
	2	7.25E-01	1.76E+00
	5	6.86E-01	1.66E+00
	10	6.50E-01	1.57E+00
2	**0**	1.01E+00	4.11E+00
	0.5	8.73E-01	3.55E+00
	1	7.88E-01	3.19E+00
	2	7.21E-01	2.88E+00
	5	6.81E-01	2.63E+00
	10	6.46E-01	2.47E+00
5	**0**	1.01E+00	1.97E+00
	0.5	8.67E-01	1.74E+00
	1	7.83E-01	1.59E+00
	2	7.16E-01	1.41E+00
	5	6.77E-01	1.22E+00
	10	6.42E-01	1.12E+00
10	**0**	1.00E+00	1.01E+00
	0.5	8.65E-01	8.86E-01
	1	7.81E-01	8.10E-01
	2	7.15E-01	7.23E-01
	5	6.24E-01	6.75E-01
	10	5.74E-01	6.41E-01

The first and the second natural frequencies of untwisted (ψ=0) $\boldsymbol{Al/Al_2O_3}$ FGM plates for different combinations of aspect ratio (a/b) and power index values (k) are given in **Table 3.8(a)**, **Table 3.8(b)**, **Table 3.8(c)** and **Table 3.8(d)** for porosity types 0,1,2 and 3 respectively. The aspect ratio values are varied as 1,2,5 and 10 while the power index values are varied from 1 to 10. In general, the first natural frequencies are always found to be lower than the second natural frequency values. For a certain value of the power index k, the maximum value of the first natural frequencies is observed for the square plate (a/b=1) and decreases with an increase in the aspect ratio for all the porosity types. For example, at k=2, the fundamental frequencies are 7.20E-01, 7.12E-01, 7.03E-01 and 7.00E-01 for the aspect ratios considered for the plate with no porosity (**Table 3.8(a)**). This clear trend of decrease in the natural frequency values is due to the fact that the stiffness of the plate decreases with an increase in the aspect ratio. However, for a particular porosity type, the second natural frequency is initially increases as the aspect ratio is increased from 1 to 2 and thereafter decreases with increase in the aspect ratio values for 5 and 10. For a particular aspect ratio in case of untwisted plates, both the first and second natural frequencies are found to decrease with an increase in the power index values for the range of the values considered (k=1 to 10). As evident, the contribution of the metallic constituents predominates with an increase in the power index value (k). As in this case the ceramic constituent Al_2O_3 with E=380 GPa has high strength compared to the metallic part Aluminium (Al) which is extremely soft with E=70 GPa. Thus, an increase in the power index results in a decrease in the natural frequency values owing to the weakness due to transition towards the metallic properties. From **Table 3.8** it can be inferred that the highest values of the first natural frequency for $\boldsymbol{Al/Al_2O_3}$ FGM plate is observed for porosity type 1 while the lowest value is observed for porosity type 2. For the second natural frequencies, the values are highest and lowest for porosity type 1 and 0 respectively.

FGM 2: $SUS304/Si_3N_4$

Table 3.9(a) *The first and the second natural frequencies of untwisted(ψ=0) SUS304/Si_3N_4 FGM plates for different aspect ratios(a/b) and power index values (k) for no porosity(type o)*

		Porosity Type 0	
Aspect Ratio	**k**	**1st Freq.**	**2nd Freq.**
1	**0**	1.03E+00	2.48E+00
	0.5	7.13E-01	1.70E+00
	1	6.25E-01	1.48E+00
	2	5.61E-01	1.32E+00
	5	5.10E-01	1.20E+00
	10	4.85E-01	1.14E+00
2	**0**	1.02E+00	4.09E+00
	0.5	7.06E-01	2.80E+00
	1	6.18E-01	2.44E+00
	2	5.55E-01	2.18E+00
	5	5.04E-01	1.97E+00
	10	4.80E-01	1.87E+00
5	**0**	1.01E+00	1.97E+00
	0.5	6.99E-01	1.38E+00
	1	6.12E-01	1.20E+00
	2	5.49E-01	1.06E+00
	5	4.98E-01	9.49E-01
	10	4.74E-01	9.03E-01
10	**0**	1.01E+00	1.01E+00
	0.5	6.97E-01	7.04E-01
	1	6.10E-01	6.13E-01
	2	5.43E-01	5.47E-01
	5	4.85E-01	4.96E-01
	10	4.61E-01	4.72E-01

Table 3.9(b) *The first and the second natural frequencies of untwisted(ψ=0) SUS304/Si_3N_4FGM plates for different aspect ratios(a/b) and power index values (k) for Porosity type 1*

		Porosity Type 1	
Aspect Ratio	**k**	**1st Freq.**	**2nd Freq.**
1	**0**	1.11E+00	2.72E+00
	0.5	7.66E-01	1.85E+00
	1	6.75E-01	1.62E+00
	2	6.12E-01	1.47E+00
	5	5.60E-01	1.34E+00
	10	5.31E-01	1.27E+00

		Porosity Type 1	
Aspect Ratio	**k**	**1st Freq.**	**2nd Freq.**
2	**0**	1.11E+00	4.38E+00
	0.5	7.61E-01	3.00E+00
	1	6.71E-01	2.63E+00
	2	6.08E-01	2.36E+00
	5	5.55E-01	2.13E+00
	10	5.27E-01	2.02E+00
5	**0**	1.10E+00	1.98E+00
	0.5	7.56E-01	1.37E+00
	1	6.66E-01	1.20E+00
	2	6.03E-01	1.08E+00
	5	5.51E-01	9.68E-01
	10	5.22E-01	9.17E-01
10	**0**	1.01E+00	1.10E+00
	0.5	6.99E-01	7.55E-01
	1	6.14E-01	6.64E-01
	2	5.49E-01	6.01E-01
	5	4.94E-01	5.49E-01
	10	4.68E-01	5.21E-01

Table 3.9(c) *The first and the second natural frequencies of untwisted(ψ=0) SUS304/Si_3N_4 FGM plates for different aspect ratios(a/b) and power index values (k) for Porosity type 2*

		Porosity Type 2	
Aspect Ratio	**k**	**1st Freq.**	**2nd Freq.**
1	**0**	1.01E+00	2.51E+00
	0.5	7.23E-01	1.78E+00
	1	6.33E-01	1.56E+00
	2	5.66E-01	1.39E+00
	5	5.09E-01	1.25E+00
	10	4.81E-01	1.17E+00
2	**0**	1.01E+00	4.16E+00
	0.5	7.20E-01	2.95E+00
	1	6.31E-01	2.57E+00
	2	5.63E-01	2.29E+00
	5	5.07E-01	2.05E+00
	10	4.79E-01	1.93E+00
5	**0**	1.01E+00	1.98E+00
	0.5	7.17E-01	1.44E+00
	1	6.27E-01	1.26E+00
	2	5.60E-01	1.11E+00
	5	5.04E-01	9.81E-01
	10	4.76E-01	9.21E-01

		Porosity Type 2	
Aspect Ratio	k	1st Freq.	2nd Freq.
10	0	1.00E+00	1.01E+00
	0.5	7.16E-01	7.35E-01
	1	6.26E-01	6.44E-01
	2	5.59E-01	5.69E-01
	5	5.01E-01	5.03E-01
	10	4.70E-01	4.75E-01

Table 3.9(d) *The first and the second natural frequencies of untwisted(ψ=0) SUS304/Si_3N_4 FGM plates for different aspect ratios(a/b) and power index values (k) for Porosity type 3*

		Porosity Type 3	
Aspect Ratio	k	1st Freq.	2nd Freq.
1	0	1.01E+00	2.51E+00
	0.5	6.80E-01	1.67E+00
	1	5.97E-01	1.46E+00
	2	5.40E-01	1.31E+00
	5	4.95E-01	1.20E+00
	10	4.73E-01	1.15E+00
2	0	1.01E+00	4.16E+00
	0.5	6.77E-01	2.77E+00
	1	5.93E-01	2.42E+00
	2	5.37E-01	2.18E+00
	5	4.92E-01	1.99E+00
	10	4.70E-01	1.90E+00
5	0	1.01E+00	1.98E+00
	0.5	6.73E-01	1.32E+00
	1	5.90E-01	1.15E+00
	2	5.33E-01	1.02E+00
	5	4.89E-01	9.26E-01
	10	4.67E-01	8.90E-01
10	0	1.00E+00	1.01E+00
	0.5	6.72E-01	6.73E-01
	1	5.85E-01	5.89E-01
	2	5.21E-01	5.32E-01
	5	4.73E-01	4.88E-01
	10	4.54E-01	4.66E-01

The first and the second natural frequencies of untwisted (ψ=0) ***SUS304/Si_3N_4*** FGM plates for different combinations of aspect ratio (*a/b*) and power index values (*k*) are given in **Table 3.9(a)**, **Table 3.9(b)**, **Table 3.9(c)** and **Table 3.9(d)** for porosity types 0,1,2 and 3 respectively. The aspect ratio values are varied as 1,2,5 and 10 while the power index values are varied from 1 to 10. In general, the first natural frequencies are always found to be lower than the second natural frequency values. For a certain value of the power index *k*, the maximum value

of the first natural frequencies is observed for the square plate (a/b=1) and decreases with an increase in the aspect ratio. For example, at k=5, the fundamental frequencies are 5.10E-01, 5.04E-01, 4.98E-01 and 4.85E-01 for the aspect ratios considered for the plate with no porosity (**Table 3.9(a)**). This clear trend of decrease in the natural frequency values is due to the fact that the stiffness of the plate decreases with an increase in the aspect ratio. However, the second natural frequency is highest for aspect ratio 2 and lowest for highest ratio 10. In case of both twisted and untwisted plates, both the first and second natural frequencies are found to decrease with an increase in the power index value for the range of the values considered (k=1 to 10). As evident, the contribution of the metallic constituents predominates with an increase in the power index value (k). As in this case the ceramic constituent silicon nitride (Si_3N_4) with E=322.27 GPa has high strength compared to the metallic part stainless steel (SUS304) which is softer with E=207.78 GPa. Thus, an increase in the power index results in a decrease in the natural frequency values owing to the weakness due to transition towards the metallic properties. Furthermore, from **Table 3.9** it can be inferred that the highest values of both the first and second natural frequencies for $\boldsymbol{SUS304/Si_3N_4}$ FGM plate is observed for porosity type 1 while the lowest value is observed for porosity type 3.

FGM 3: *Ti-6Al-4V/Aluminium Oxide*

Table 3.10(a) *The first and the second natural frequencies of untwisted(ψ=0) Ti-6Al-4V/Aluminium Oxide FGM plates for different aspect ratios(a/b) and power index values (k) for no porosity(Type 0)*

		Porosity Type 0	
Aspect Ratio	**k**	**1st Freq.**	**2nd Freq.**
1	**0**	1.03E+00	2.46E+00
	0.5	8.55E-01	2.04E+00
	1	7.74E-01	1.84E+00
	2	7.11E-01	1.68E+00
	5	6.64E-01	1.57E+00
	10	6.31E-01	1.49E+00

		Porosity Type 0	
Aspect Ratio	**k**	**1st Freq.**	**2nd Freq.**
2	**0**	1.02E+00	4.07E+00
	0.5	8.47E-01	3.35E+00
	1	7.66E-01	3.02E+00
	2	7.04E-01	2.75E+00
	5	6.57E-01	2.54E+00
	10	6.25E-01	2.41E+00
5	**0**	1.01E+00	1.97E+00
	0.5	8.38E-01	1.69E+00
	1	7.58E-01	1.54E+00
	2	6.96E-01	1.39E+00
	5	6.50E-01	1.22E+00
	10	6.17E-01	1.14E+00
10	**0**	1.01E+00	1.01E+00
	0.5	8.36E-01	8.64E-01
	1	7.55E-01	7.87E-01
	2	6.94E-01	7.08E-01
	5	6.23E-01	6.47E-01
	10	5.82E-01	6.15E-01

Table 3.10(b) *The first and the second natural frequencies of untwisted(ψ=0) Ti-6Al-4V/Aluminium Oxide FGM plates for different aspect ratios(a/b) and power index values (k) for porosity type 1*

		Porosity Type 1	
Aspect Ratio	**k**	**1st Freq.**	**2nd Freq.**
1	**0**	1.12E+00	2.71E+00
	0.5	9.19E-01	2.22E+00
	1	8.30E-01	2.00E+00
	2	7.67E-01	1.85E+00
	5	7.22E-01	1.73E+00
	10	6.89E-01	1.65E+00
2	**0**	1.11E+00	4.38E+00
	0.5	9.13E-01	3.61E+00
	1	8.25E-01	3.25E+00
	2	7.62E-01	2.96E+00
	5	7.17E-01	2.71E+00
	10	6.84E-01	2.56E+00
5	**0**	1.10E+00	1.98E+00
	0.5	9.07E-01	1.69E+00
	1	8.19E-01	1.54E+00
	2	7.56E-01	1.40E+00
	5	7.11E-01	1.25E+00
	10	6.78E-01	1.17E+00

		Porosity Type 1	
Aspect Ratio	**k**	**1st Freq.**	**2nd Freq.**
10	**0**	1.01E+00	1.10E+00
	0.5	8.60E-01	9.05E-01
	1	7.88E-01	8.17E-01
	2	7.16E-01	7.54E-01
	5	6.39E-01	7.10E-01
	10	5.95E-01	6.77E-01

Table 3.10(c) *The first and the second natural frequencies of untwisted(ψ=0) Ti-6Al-4V/Aluminium Oxide FGM plates for different aspect ratios(a/b) and power index values (k) for porosity type 2*

		Porosity Type 2	
Aspect Ratio	**k**	**1st Freq.**	**2nd Freq.**
1	**0**	1.02E+00	2.50E+00
	0.5	8.42E-01	2.07E+00
	1	7.60E-01	1.87E+00
	2	6.94E-01	1.71E+00
	5	6.47E-01	1.59E+00
	10	6.19E-01	1.51E+00
2	**0**	1.01E+00	4.14E+00
	0.5	8.38E-01	3.42E+00
	1	7.56E-01	3.08E+00
	2	6.91E-01	2.80E+00
	5	6.44E-01	2.58E+00
	10	6.16E-01	2.46E+00
5	**0**	1.01E+00	1.98E+00
	0.5	8.34E-01	1.73E+00
	1	7.52E-01	1.60E+00
	2	6.87E-01	1.45E+00
	5	6.41E-01	1.27E+00
	10	6.12E-01	1.17E+00
10	**0**	1.00E+00	1.01E+00
	0.5	8.32E-01	8.85E-01
	1	7.51E-01	8.16E-01
	2	6.86E-01	7.39E-01
	5	6.40E-01	6.49E-01
	10	5.99E-01	6.11E-01

Table 3.10(d) *The first and the second natural frequencies of untwisted(ψ=0) Ti-6Al-4V/Aluminium Oxide FGM plates for different aspect ratios(a/b) and power index values (k) for porosity type 3*

		Porosity Type 3	
Aspect Ratio	**k**	**1st Freq.**	**2nd Freq.**
1	**0**	1.02E+00	2.50E+00
	0.5	8.41E-01	2.06E+00
	1	7.62E-01	1.87E+00
	2	7.05E-01	1.72E+00
	5	6.58E-01	1.60E+00
	10	6.21E-01	1.51E+00
2	**0**	1.01E+00	4.14E+00
	0.5	8.37E-01	3.42E+00
	1	7.59E-01	3.08E+00
	2	7.01E-01	2.82E+00
	5	6.54E-01	2.59E+00
	10	6.18E-01	2.46E+00
5	**0**	1.01E+00	1.98E+00
	0.5	8.32E-01	1.65E+00
	1	7.54E-01	1.48E+00
	2	6.97E-01	1.33E+00
	5	6.50E-01	1.18E+00
	10	6.14E-01	1.12E+00
10	**0**	1.00E+00	1.01E+00
	0.5	8.31E-01	8.41E-01
	1	7.53E-01	7.58E-01
	2	6.78E-01	6.95E-01
	5	6.03E-01	6.49E-01
	10	5.70E-01	6.13E-01

FGM 4: Al/ZrO_2

Table 3.11(a) *The first and the second natural frequencies of untwisted(ψ=0) Al/ZrO_2 FGM plates for different aspect ratios(a/b) and power index values (k) for no porosity (Type 0)*

		Porosity Type 0	
Aspect Ratio	**k**	**1st Freq.**	**2nd Freq.**
1	**0**	1.04E+00	2.44E+00
	0.5	9.36E-01	2.20E+00
	1	8.91E-01	2.09E+00
	2	8.59E-01	2.02E+00
	5	8.32E-01	1.95E+00
	10	8.08E-01	1.89E+00

		Porosity Type 0	
Aspect Ratio	**k**	**1st Freq.**	**2nd Freq.**
2	**0**	1.03E+00	4.02E+00
	0.5	9.26E-01	3.62E+00
	1	8.81E-01	3.44E+00
	2	8.49E-01	3.30E+00
	5	8.23E-01	3.19E+00
	10	7.98E-01	3.10E+00
5	**0**	1.01E+00	1.97E+00
	0.5	9.14E-01	1.82E+00
	1	8.70E-01	1.73E+00
	2	8.38E-01	1.64E+00
	5	8.12E-01	1.53E+00
	10	7.88E-01	1.48E+00
10	**0**	1.01E+00	1.01E+00
	0.5	9.10E-01	9.29E-01
	1	8.66E-01	8.84E-01
	2	8.35E-01	8.36E-01
	5	7.82E-01	8.09E-01
	10	7.55E-01	7.85E-01

Table 3.11(b) *The first and the second natural frequencies of untwisted(ψ=0) Al/ZrO_2 FGM plates for different aspect ratios(a/b) and power index values (k) for porosity type 1*

		Porosity Type 1	
Aspect Ratio	**k**	**1st Freq.**	**2nd Freq.**
1	**0**	1.12E+00	2.68E+00
	0.5	1.01E+00	2.41E+00
	1	9.59E-01	2.29E+00
	2	9.27E-01	2.21E+00
	5	9.02E-01	2.15E+00
	10	8.77E-01	2.09E+00
2	**0**	1.11E+00	4.37E+00
	0.5	1.00E+00	3.93E+00
	1	9.51E-01	3.72E+00
	2	9.19E-01	3.56E+00
	5	8.95E-01	3.40E+00
	10	8.70E-01	3.29E+00
5	**0**	1.10E+00	1.98E+00
	0.5	9.92E-01	1.82E+00
	1	9.43E-01	1.73E+00
	2	9.12E-01	1.65E+00
	5	8.87E-01	1.55E+00
	10	8.63E-01	1.50E+00

		Porosity Type 1	
Aspect Ratio	**k**	**1st Freq.**	**2nd Freq.**
10	**0**	1.01E+00	1.10E+00
	0.5	9.28E-01	9.89E-01
	1	8.85E-01	9.41E-01
	2	8.41E-01	9.09E-01
	5	7.92E-01	8.85E-01
	10	7.64E-01	8.61E-01

Table 3.11(c) *The first and the second natural frequencies of untwisted(ψ=0) Al/ZrO_2 FGM plates for different aspect ratios(a/b) and power index values (k) for porosity type 2*

		Porosity Type 2	
Aspect Ratio	**k**	**1st Freq.**	**2nd Freq.**
1	**0**	1.02E+00	2.48E+00
	0.5	9.14E-01	2.23E+00
	1	8.67E-01	2.12E+00
	2	8.33E-01	2.03E+00
	5	8.09E-01	1.97E+00
	10	7.90E-01	1.92E+00
2	**0**	1.01E+00	4.11E+00
	0.5	9.09E-01	3.68E+00
	1	8.62E-01	3.49E+00
	2	8.28E-01	3.34E+00
	5	8.05E-01	3.23E+00
	10	7.86E-01	3.15E+00
5	**0**	1.01E+00	1.97E+00
	0.5	9.03E-01	1.84E+00
	1	8.57E-01	1.76E+00
	2	8.23E-01	1.67E+00
	5	8.00E-01	1.56E+00
	10	7.81E-01	1.50E+00
10	**0**	1.00E+00	1.01E+00
	0.5	9.01E-01	9.41E-01
	1	8.55E-01	9.01E-01
	2	8.22E-01	8.55E-01
	5	7.98E-01	7.99E-01
	10	7.65E-01	7.79E-01

Table 3.11(d) *The first and the second natural frequencies of untwisted(ψ=0) Al/ZrO_2 FGM plates for different aspect ratios(a/b) and power index values (k) for porosity type 3*

		Porosity Type 3	
Aspect Ratio	**k**	**1st Freq.**	**2nd Freq.**
1	**0**	1.02E+00	2.48E+00
	0.5	9.24E-01	2.25E+00
	1	8.82E-01	2.15E+00
	2	8.52E-01	2.07E+00
	5	8.23E-01	2.00E+00
	10	7.94E-01	1.93E+00
2	**0**	1.01E+00	4.11E+00
	0.5	9.19E-01	3.73E+00
	1	8.77E-01	3.56E+00
	2	8.48E-01	3.42E+00
	5	8.18E-01	3.30E+00
	10	7.90E-01	3.19E+00
5	**0**	1.01E+00	1.97E+00
	0.5	9.13E-01	1.79E+00
	1	8.71E-01	1.70E+00
	2	8.42E-01	1.60E+00
	5	8.13E-01	1.51E+00
	10	7.85E-01	1.46E+00
10	**0**	1.00E+00	1.01E+00
	0.5	9.11E-01	9.16E-01
	1	8.66E-01	8.70E-01
	2	8.17E-01	8.40E-01
	5	7.68E-01	8.11E-01
	10	7.47E-01	7.83E-01

The same trend of decreasing first natural frequency with increasing aspect ratio is seen in ***Ti-6Al-4V/Aluminium Oxide*** and ***Al/ZrO_2*** FG plates as previously seen in FGM 1 and FGM 2, irrespective of porosity type. The second natural frequency is highest for aspect ratio 2 and lowest for highest ratio 10 for both the plates. Also, both the first and second natural frequencies are found to decrease with an increase in the power index value for the range of the values considered (k=1 to 10), for both twisted and untwisted plates.

However, from **Table 3.10** and **Table 3.11** it can be inferred that the highest values of the first natural frequencies for both ***Ti-6Al-4V/Aluminium Oxide*** and ***Al/ZrO_2*** FGM plates are observed for porosity type 1 while the lowest value is observed for porosity type 2. The second natural frequencies for both the plates are highest at porosity type 1 and lowest at porosity type 0.

3.3.3 Influence of varying non-dimensional rotational speed $\left(\Delta_r = \frac{\omega}{\omega_0}\right)$ for different Porosity Types

In this study, the non-dimensional rotational speed $\Delta_r = \frac{\omega}{\omega_0}$ is considered wherein ω is the actual speed of rotation, while ω_0 is the circular frequency at resonance which is obtained from the FEM code. The Δ_r is varied from $\Delta_r = 0$ (no rotation) to 50% of the circular frequency at resonance (Δ_r=0.5).

FGM 1: Al/Al_2O_3

Table 3.12(a) *The first natural frequency values of untwisted(ψ=0) Al/Al_2O_3 FGM plates for different rotational speeds(ω) with varying power index values (k) and porosity type*

		1st NF					
Porosity Type	***k***	Δ_r***=0***	Δ_r***=0.1***	Δ_r***=0.2***	Δ_r***=0.3***	Δ_r***=0.4***	Δ_r***=0.5***
0	***0***	1.04E+00	1.04E+00	1.05E+00	1.06E+00	1.07E+00	1.09E+00
	0.5	8.84E-01	8.83E-01	8.87E-01	8.94E-01	9.05E-01	9.18E-01
	1	7.95E-01	7.95E-01	7.99E-01	8.05E-01	8.15E-01	8.26E-01
	2	7.20E-01	7.22E-01	7.26E-01	7.32E-01	7.41E-01	7.52E-01
	5	6.79E-01	6.83E-01	6.87E-01	6.93E-01	7.02E-01	7.13E-01
	10	6.52E-01	6.60E-01	6.64E-01	6.71E-01	6.87E-01	6.90E-01
1	***0***	1.12E+00	1.12E+00	1.13E+00	1.15E+00	1.17E+00	1.20E+00
	0.5	9.46E-01	9.47E-01	9.48E-01	9.59E-01	9.74E-01	9.93E-01
	1	8.43E-01	8.44E-01	8.47E-01	8.57E-01	8.71E-01	8.88E-01
	2	7.64E-01	7.65E-01	7.71E-01	7.80E-01	7.93E-01	8.09E-01
	5	7.27E-01	7.37E-01	7.37E-01	7.46E-01	7.59E-01	7.75E-01
	10	7.05E-01	7.13E-01	7.19E-01	7.28E-01	7.44E-01	7.57E-01
2	***0***	1.02E+00	1.02E+00	1.03E+00	1.03E+00	1.04E+00	1.06E+00
	0.5	8.59E-01	8.60E-01	8.63E-01	8.69E-01	8.75E-01	8.82E-01
	1	7.67E-01	7.69E-01	7.21E-01	7.48E-01	7.78E-01	7.89E-01
	2	6.88E-01	6.90E-01	6.94E-01	6.98E-01	7.04E-01	7.11E-01
	5	6.45E-01	6.49E-01	6.51E-01	6.57E-01	6.64E-01	6.70E-01
	10	6.27E-01	6.35E-01	6.38E-01	6.42E-01	6.49E-01	6.56E-01
3	***0***	1.02E+00	1.02E+00	1.03E+00	1.05E+00	1.07E+00	1.09E+00
	0.5	8.78E-01	8.76E-01	8.83E-01	8.93E-01	9.27E-01	9.27E-01
	1	7.93E-01	7.93E-01	7.99E-01	8.09E-01	8.23E-01	8.40E-01
	2	7.25E-01	7.29E-01	7.34E-01	7.44E-01	7.56E-01	7.73E-01
	5	6.86E-01	6.91E-01	6.97E-01	7.06E-01	7.19E-01	7.35E-01
	10	6.50E-01	6.59E-01	6.64E-01	6.73E-01	6.86E-01	7.06E-01

Table 3.12(b) *The second natural frequency values of untwisted(ψ=0) Al/Al_2O_3 FGM plates for different rotational speeds(ω) with varying power index values (k) and porosity types*

		2nd NF					
Porosity Type	***k***	Δ_r***=0***	Δ_r***=0.1***	Δ_r***=0.2***	Δ_r***=0.3***	Δ_r***=0.4***	Δ_r***=0.5***
0	***0***	2.44E+00	2.44E+00	2.45E+00	2.47E+00	2.48E+00	2.51E+00
	0.5	2.08E+00	2.08E+00	2.08E+00	2.09E+00	2.11E+00	2.12E+00
	1	1.87E+00	1.87E+00	1.88E+00	1.89E+00	1.90E+00	1.91E+00
	2	1.70E+00	1.70E+00	1.70E+00	1.71E+00	1.72E+00	1.74E+00
	5	1.59E+00	1.60E+00	1.61E+00	1.61E+00	1.63E+00	1.64E+00
	10	1.53E+00	1.54E+00	1.55E+00	1.56E+00	1.57E+00	1.58E+00
1	***0***	2.68E+00	2.69E+00	2.70E+00	2.72E+00	2.75E+00	2.79E+00
	0.5	2.27E+00	2.26E+00	2.27E+00	2.29E+00	2.31E+00	2.33E+00
	1	2.03E+00	2.03E+00	2.04E+00	2.05E+00	2.07E+00	2.09E+00
	2	1.84E+00	1.84E+00	1.85E+00	1.86E+00	1.88E+00	1.90E+00
	5	1.74E+00	1.76E+00	1.76E+00	1.77E+00	1.79E+00	1.81E+00
	10	1.68E+00	1.70E+00	1.71E+00	1.72E+00	1.72E+00	1.76E+00
2	***0***	2.48E+00	2.49E+00	2.49E+00	2.50E+00	2.52E+00	2.53E+00
	0.5	2.10E+00	2.10E+00	2.11E+00	2.13E+00	2.14E+00	2.15E+00
	1	1.88E+00	1.88E+00	1.89E+00	1.90E+00	1.91E+00	1.91E+00
	2	1.69E+00	1.69E+00	1.70E+00	1.71E+00	1.72E+00	1.72E+00
	5	1.58E+00	1.59E+00	1.60E+00	1.61E+00	1.62E+00	1.62E+00
	10	1.53E+00	1.55E+00	1.56E+00	1.57E+00	1.57E+00	1.57E+00
3	***0***	2.48E+00	2.49E+00	2.50E+00	2.52E+00	2.55E+00	2.58E+00
	0.5	2.14E+00	2.14E+00	2.14E+00	2.16E+00	2.20E+00	2.20E+00
	1	1.93E+00	1.93E+00	1.94E+00	1.95E+00	1.97E+00	1.99E+00
	2	1.76E+00	1.77E+00	1.78E+00	1.79E+00	1.81E+00	1.83E+00
	5	1.66E+00	1.67E+00	1.68E+00	1.69E+00	1.71E+00	1.73E+00
	10	1.57E+00	1.59E+00	1.60E+00	1.61E+00	1.63E+00	1.65E+00

The first and second natural frequencies of square ***Al/Al_2O_3*** FGM plates for different combinations of non-dimensional rotational speeds (Δ_r) with varying power index values (k) and porosity types are presented in **Table 3.12(a)** and **Table 3.12(b)**. The non-dimensional rotational speeds are varied from 0 to 0.5 at a step of 0.1 while the power index values are varied from 1 to 10. For a certain value of the power index k, both the first and the second natural frequencies are found to increase with an increase in the non-dimensional rotational speeds (Δ_r) at all the porosity types considered. For example, in porosity type 1, for k=0 the first natural frequencies are 1.12E+00, 1.12E+00, 1.13E+00, 1.15E+00, 1.17E+00 and 1.20E+00 respectively for Δ_r=0 to 0.5. This increase in the natural frequencies may be attributed to the fact that there is a gradual increase in the

structural stiffness of the FGM plate owing to centrifugal stiffening effect with increase in rotation. This increase in the stiffness results in higher values of the natural frequencies obtained. Since the increase in stiffness are independent of the presence of porosity in the rotating structure, as such the rise in the natural frequency values is observed for all the porosity types considered. The increase in the first natural frequency values is found to be higher at higher power index values(k=10) compared to the lower ones(k=0). For example, the rise in the frequency values is 0.05 at k=0, while it is 0.38 at k=10. However, in case of second natural frequencies the rise in the same is not quite significant. Furthermore, the increase in the natural frequency values with rotation is found to be independent of the power index values(k). Same trend is observed for the following FG plates.

FGM 2: $SUS304/Si_3N_4$

Table 3.13(a) *The first natural frequency values of untwisted(ψ=0) SUS304/Si_3N_4 FGM plates for different rotational speeds(ω) with varying power index values (k) and porosity types*

		1st NF					
Porosity Type	***k***	Δ_r ***=0***	Δ_r ***=0.1***	Δ_r ***=0.2***	Δ_r ***=0.3***	Δ_r ***=0.4***	Δ_r ***=0.5***
0	***0***	1.03E+00	1.03E+00	1.04E+00	1.05E+00	1.06E+00	1.07E+00
	0.5	7.13E-01	7.15E-01	7.22E-01	7.33E-01	7.49E-01	7.68E-01
	1	6.25E-01	6.29E-01	6.32E-01	6.41E-01	6.54E-01	6.70E-01
	2	5.61E-01	5.63E-01	5.67E-01	5.74E-01	5.84E-01	5.97E-01
	5	5.10E-01	5.11E-01	5.15E-01	5.21E-01	5.29E-01	5.39E-01
	10	4.85E-01	4.86E-01	4.90E-01	4.95E-01	5.02E-01	5.11E-01
1	***0***	1.11E+00	1.12E+00	1.13E+00	1.14E+00	1.16E+00	1.19E+00
	0.5	7.66E-01	7.69E-01	7.79E-01	7.95E-01	8.17E-01	8.45E-01
	1	6.75E-01	6.78E-01	6.86E-01	7.00E-01	7.18E-01	7.41E-01
	2	6.12E-01	6.14E-01	6.21E-01	6.32E-01	6.46E-01	6.65E-01
	5	5.60E-01	5.61E-01	5.67E-01	5.75E-01	5.87E-01	6.02E-01
	10	5.31E-01	5.33E-01	5.39E-01	5.48E-01	5.56E-01	5.69E-01
2	***0***	1.01E+00	1.01E+00	1.02E+00	1.03E+00	1.04E+00	1.05E+00
	0.5	7.23E-01	7.25E-01	7.30E-01	7.40E-01	7.52E-01	7.68E-01
	1	6.33E-01	6.35E-01	6.39E-01	6.47E-01	6.57E-01	6.70E-01
	2	5.66E-01	5.67E-01	5.70E-01	5.76E-01	5.84E-01	5.94E-01
	5	5.09E-01	5.10E-01	5.13E-01	5.17E-01	5.23E-01	5.31E-01
	10	4.81E-01	4.82E-01	4.85E-01	4.88E-01	4.94E-01	5.01E-01
3	***0***	1.01E+00	1.02E+00	1.02E+00	1.04E+00	1.06E+00	1.08E+00
	0.5	6.80E-01	6.83E-01	6.92E-01	7.06E-01	7.25E-01	7.49E-01
	1	5.97E-01	5.99E-01	6.07E-01	6.17E-01	6.31E-01	6.53E-01
	2	5.40E-01	5.41E-01	5.47E-01	5.56E-01	5.69E-01	5.85E-01
	5	4.95E-01	4.96E-01	5.01E-01	5.09E-01	5.19E-01	5.32E-01
	10	4.73E-01	4.74E-01	4.78E-01	4.85E-01	4.95E-01	5.07E-01

Table 3.13(b) *The second natural frequency values of untwisted(ψ=0) SUS304/Si_3N_4 FGM plates for different rotational speeds(ω) with varying power index values (k) and porosity types*

		2nd NF					
Porosity Type	***k***	Δ_r***=0***	Δ_r***=0.1***	Δ_r***=0.2***	Δ_r***=0.3***	Δ_r***=0.4***	Δ_r***=0.5***
0	***0***	2.48E+00	2.48E+00	2.49E+00	2.50E+00	2.52E+00	2.54E+00
	0.5	1.70E+00	1.70E+00	1.71E+00	1.73E+00	1.75E+00	1.77E+00
	1	1.48E+00	1.48E+00	1.49E+00	1.50E+00	1.52E+00	1.54E+00
	2	1.32E+00	1.33E+00	1.33E+00	1.34E+00	1.36E+00	1.37E+00
	5	1.20E+00	1.20E+00	1.21E+00	1.21E+00	1.22E+00	1.24E+00
	10	1.14E+00	1.14E+00	1.14E+00	1.15E+00	1.16E+00	1.17E+00
1	***0***	2.72E+00	2.72E+00	2.73E+00	2.75E+00	2.78E+00	2.82E+00
	0.5	1.85E+00	1.86E+00	1.87E+00	1.89E+00	1.92E+00	1.96E+00
	1	1.62E+00	1.63E+00	1.64E+00	1.66E+00	1.68E+00	1.71E+00
	2	1.47E+00	1.47E+00	1.48E+00	1.49E+00	1.51E+00	1.54E+00
	5	1.34E+00	1.34E+00	1.35E+00	1.36E+00	1.38E+00	1.40E+00
	10	1.27E+00	1.28E+00	1.29E+00	1.29E+00	1.30E+00	1.32E+00
2	***0***	2.51E+00	2.51E+00	2.52E+00	2.53E+00	2.54E+00	2.56E+00
	0.5	1.78E+00	1.79E+00	1.79E+00	1.81E+00	1.82E+00	1.84E+00
	1	1.56E+00	1.56E+00	1.57E+00	1.58E+00	1.59E+00	1.61E+00
	2	1.39E+00	1.39E+00	1.40E+00	1.40E+00	1.41E+00	1.43E+00
	5	1.25E+00	1.25E+00	1.25E+00	1.26E+00	1.26E+00	1.27E+00
	10	1.17E+00	1.18E+00	1.18E+00	1.18E+00	1.19E+00	1.20E+00
3	***0***	2.51E+00	2.52E+00	2.53E+00	2.55E+00	2.57E+00	2.60E+00
	0.5	1.67E+00	1.67E+00	1.68E+00	1.70E+00	1.73E+00	1.76E+00
	1	1.46E+00	1.46E+00	1.47E+00	1.49E+00	1.52E+00	1.55E+00
	2	1.31E+00	1.32E+00	1.32E+00	1.34E+00	1.35E+00	1.37E+00
	5	1.20E+00	1.21E+00	1.21E+00	1.22E+00	1.24E+00	1.25E+00
	10	1.15E+00	1.15E+00	1.16E+00	1.17E+00	1.18E+00	1.19E+00

FGM 3: *Ti-6Al-4V/Aluminium Oxide*

Table 3.14(a) *The first natural frequency values of untwisted(ψ=0) Ti-6Al-4V/Aluminium Oxide FGM plates for different rotational speeds(ω) with varying power index values (k) and porosity types*

		1st NF					
Porosity Type	***k***	Δ_r ***=0***	Δ_r ***=0.1***	Δ_r ***=0.2***	Δ_r ***=0.3***	Δ_r ***=0.4***	Δ_r ***=0.5***
0	***0***	1.03E+00	1.03E+00	1.04E+00	1.05E+00	1.06E+00	1.08E+00
	0.5	8.55E-01	8.57E-01	8.63E-01	8.72E-01	8.85E-01	9.01E-01
	1	7.74E-01	7.76E-01	7.81E-01	7.89E-01	8.00E-01	8.15E-01
	2	7.11E-01	7.13E-01	7.17E-01	7.25E-01	7.35E-01	7.48E-01
	5	6.64E-01	6.66E-01	6.70E-01	6.76E-01	6.86E-01	6.98E-01
	10	6.31E-01	6.33E-01	6.36E-01	6.43E-01	6.52E-01	6.63E-01
1	***0***	1.12E+00	1.12E+00	1.13E+00	1.14E+00	1.16E+00	1.19E+00
	0.5	9.19E-01	9.22E-01	9.30E-01	9.43E-01	9.61E-01	9.84E-01
	1	8.30E-01	8.33E-01	8.40E-01	8.52E-01	8.68E-01	8.89E-01
	2	7.67E-01	7.69E-01	7.76E-01	7.87E-01	8.01E-01	8.20E-01
	5	7.22E-01	7.24E-01	7.30E-01	7.40E-01	7.54E-01	7.71E-01
	10	6.89E-01	6.91E-01	6.96E-01	7.06E-01	7.19E-01	7.35E-01
2	***0***	1.02E+00	1.02E+00	1.02E+00	1.03E+00	1.04E+00	1.05E+00
	0.5	8.42E-01	8.43E-01	8.47E-01	8.54E-01	8.63E-01	8.75E-01
	1	7.60E-01	7.61E-01	7.64E-01	7.71E-01	7.79E-01	7.90E-01
	2	6.94E-01	6.95E-01	6.99E-01	7.04E-01	7.12E-01	7.21E-01
	5	6.47E-01	6.48E-01	6.51E-01	6.56E-01	6.63E-01	6.72E-01
	10	6.19E-01	6.20E-01	6.22E-01	6.27E-01	6.34E-01	6.42E-01
3	***0***	1.02E+00	1.02E+00	1.03E+00	1.04E+00	1.06E+00	1.08E+00
	0.5	8.41E-01	8.43E-01	8.51E-01	8.64E-01	8.81E-01	9.02E-01
	1	7.62E-01	7.65E-01	7.72E-01	7.83E-01	7.99E-01	8.18E-01
	2	7.05E-01	7.07E-01	7.13E-01	7.23E-01	7.37E-01	7.55E-01
	5	6.58E-01	6.60E-01	6.65E-01	6.75E-01	6.87E-01	7.04E-01
	10	6.21E-01	6.23E-01	6.28E-01	6.37E-01	6.49E-01	6.64E-01

Table 3.14(b) *The first natural frequency values of untwisted(ψ=0) Ti-6Al-4V/Aluminium Oxide FGM plates for different rotational speeds(ω) with varying power index values (k) and porosity types*

		2nd NF					
Porosity Type	***k***	Δ_r ***=0***	Δ_r ***=0.1***	Δ_r***=0.2***	Δ_r***=0.3***	Δ_r***=0.4***	Δ_r***=0.5***
0	***0***	2.46E+00	2.47E+00	2.47E+00	2.49E+00	2.51E+00	2.53E+00
	0.5	2.04E+00	2.04E+00	2.05E+00	2.06E+00	2.07E+00	2.10E+00
	1	1.84E+00	1.84E+00	1.85E+00	1.86E+00	1.87E+00	1.89E+00
	2	1.68E+00	1.69E+00	1.69E+00	1.70E+00	1.72E+00	1.73E+00
	5	1.57E+00	1.57E+00	1.57E+00	1.58E+00	1.59E+00	1.61E+00
	10	1.49E+00	1.49E+00	1.49E+00	1.50E+00	1.51E+00	1.53E+00
1	***0***	2.71E+00	2.71E+00	2.72E+00	2.74E+00	2.77E+00	2.80E+00
	0.5	2.22E+00	2.22E+00	2.24E+00	2.25E+00	2.28E+00	2.31E+00
	1	2.00E+00	2.01E+00	2.02E+00	2.03E+00	2.06E+00	2.08E+00
	2	1.85E+00	1.85E+00	1.86E+00	1.87E+00	1.89E+00	1.92E+00
	5	1.73E+00	1.73E+00	1.74E+00	1.75E+00	1.77E+00	1.80E+00
	10	1.65E+00	1.65E+00	1.66E+00	1.67E+00	1.69E+00	1.71E+00
2	***0***	2.50E+00	2.51E+00	2.51E+00	2.52E+00	2.53E+00	2.55E+00
	0.5	2.07E+00	2.08E+00	2.08E+00	2.09E+00	2.10E+00	2.12E+00
	1	1.87E+00	1.87E+00	1.88E+00	1.89E+00	1.90E+00	1.91E+00
	2	1.71E+00	1.71E+00	1.71E+00	1.72E+00	1.73E+00	1.74E+00
	5	1.59E+00	1.59E+00	1.59E+00	1.60E+00	1.61E+00	1.62E+00
	10	1.51E+00	1.51E+00	1.52E+00	1.52E+00	1.53E+00	1.54E+00
3	***0***	2.50E+00	2.51E+00	2.52E+00	2.54E+00	2.56E+00	2.60E+00
	0.5	2.06E+00	2.07E+00	2.08E+00	2.09E+00	2.12E+00	2.14E+00
	1	1.87E+00	1.87E+00	1.88E+00	1.89E+00	1.91E+00	1.94E+00
	2	1.72E+00	1.72E+00	1.73E+00	1.74E+00	1.76E+00	1.79E+00
	5	1.60E+00	1.60E+00	1.61E+00	1.62E+00	1.64E+00	1.66E+00
	10	1.51E+00	1.51E+00	1.52E+00	1.53E+00	1.55E+00	1.57E+00

PART B: FREE VIBRATION ANALYSIS IN THERMAL ENVIRONMENT

3.4 *MODEL ASSUMPTIONS*

For this study, a simple supported square FGM plate with length(a)= breadth(b)=0.1m, and thickness(t)= 0.125*a, comprising of 2 different material combinations (*SUS304/Si_3N_4 & Ti-6Al-4V/Aluminium Oxide*) with maximum porosity of 0.5 are considered. The material properties of the metal and the ceramic constituents are evaluated using equation no 2.4.

Table 3.15 Material constants of SUS304 and Si_3N_4

Material Constants	***SUS304***			***Si_3N_4***		
	E(N/m^2)	ν	ρ(kg/m^3)	E(N/m^2)	ν	ρ(kg/m^3)
P_0	201.04 X 10^9	0.3262	8166	348.43 X 10^9	0.24	2370
P_{-1}	0	0	0	0	0	0
P_1	3.079 X 10^{-4}	-2.002 X 10^{-4}	0	-3.070 X 10^{-4}	0	0
P_2	-6.534 X 10^{-7}	3.797 X 10^{-7}	0	2.160 X 10^{-7}	0	0
P_3	0	0	0	-8.946 X 10^{-11}	0	0

Table 3.16 Material constants of Aluminium Oxide and Ti-6Al-4V

Material Constants	***Aluminium Oxide***			***Ti-6Al-4V***		
	E(N/m^2)	ν	ρ(kg/m^3)	E(N/m^2)	ν	ρ(kg/m^3)
P_0	349.55 X 10^9	0.26	3750	122.56 X 10^9	0.2884	4429
P_{-1}	0	0	0	0	0	0
P_1	-3.853 X 10^{-4}	0	0	-4.586 X 10^{-4}	1.12 X 10^{-4}	0
P_2	4.027 X 10^{-7}	0	0	0	0	0
P_3	-1.673 X 10^{-10}	0	0	0	0	0

Table 3.15 and **Table 3.16** show the values of the material constants for thermal analysis of the FGM components. For these two material combinations, free vibration characteristics of the FGM plate for different volume fractions(k) and porosity type (0,1,2 & 3) are demonstrated and discussed.

3.5 *RESULTS AND DISCUSSION OF FREE VIBRATION CHARACTERISTICS FOR DIFFERENT THERMAL GRADIENTS*

FGM: $SUS304/Si_3N_4$

Table 3.17 *The first natural frequency values of untwisted(ψ=0)* ***SUS304/Si_3N_4*** *FG plates for different temperature gradients(ΔT) with varying power index values (k) and porosity types*

		Porosity Type			
Temperature	***k***	***Type 0***	***Type 1***	***Type 2***	***Type 3***
T_m = 300 K T_c = 300K	**0**	12.241	13.176	12.234	12.234
	0.5	8.523	9.09	8.857	8.145
	1	7.486	8.029	7.808	7.131
	2	6.729	7.282	6.987	6.446
	5	6.106	6.643	6.256	5.926
	10	5.805	6.297	5.882	5.682
T_m = 300 K T_c = 400 K	**0**	12.351	13.405	12.436	12.436
	0.5	8.52	9.166	8.938	8.194
	1	7.451	8.064	7.851	7.14
	2	6.676	7.291	7.004	6.433
	5	6.036	6.63	6.248	5.894
	10	5.719	6.265	5.854	5.636
T_m = 300 K T_c = 600 K	**0**	11.514	12.736	11.794	11.794
	0.5	8.006	8.784	8.541	7.843
	1	7.035	7.761	7.534	6.867
	2	6.332	7.042	6.748	6.214
	5	5.751	6.426	6.046	5.717
	10	5.465	6.091	5.682	5.481

FGM: *Ti-6Al-4V/Aluminium Oxide*

Table 3.18 *The first natural frequency values of untwisted(ψ=0)* ***Ti-6Al-4V/Aluminium Oxide*** *FG plates for different temperature gradients(ΔT) with varying power index values (k) and porosity types*

		Porosity Type			
Temperature	**k**	**Type 0**	**Type 1**	**Type 2**	**Type 3**
T_m = 300 K T_c = 300K	**0**	10.127	10.885	10.104	10.104
	0.5	8.515	9.096	8.692	8.249
	1	7.806	8.347	8.032	7.482
	2	7.228	7.774	7.449	6.916
	5	6.665	7.225	6.846	6.421
	10	6.257	6.795	6.397	6.07
T_m = 300 K T_c = 400 K	**0**	9.715	10.531	9.767	9.767
	0.5	8.191	8.834	8.433	8.002
	1	7.533	8.132	7.816	7.282
	2	7.001	7.598	7.273	6.756
	5	6.479	7.079	6.705	6.292
	10	6.093	6.67	6.277	5.962
T_m = 300 K T_c = 600 K	**0**	9.515	10.518	9.737	9.737
	0.5	7.993	8.792	8.388	7.931
	1	7.348	8.079	7.766	7.2
	2	6.836	7.537	7.22	6.673
	5	6.327	7.011	6.648	6.21
	10	5.933	6.59	6.207	5.87

Table 3.17 and **Table 3.18** list the natural frequencies for different thermal gradients (ΔT= $T_c - T_m$) across the thickness of the FGM plate where T_c is the temperature on the ceramic(top) side and T_m is the temperature on the metal(bottom) side. The thermal gradient values considered are ΔT=0 ($T_c = 300K, T_m = 300K$), 100K ($T_c = 400K, T_m = 300K$) and 300 K ($T_c = 600K, T_m = 300K$), for different combinations of power index values (k) and porosity types.

For Ti–6Al–4V/Aluminium oxide FG plates, the first natural frequency values are found to decrease with an increase in the temperature gradient (ΔT) from 0 to 300K for all the power index (k) and porosity types. This is due to the fact that internal thermal strains (negative in nature) are developed inside the FGM plates with temperature rise which results in a decrease in the overall stiffness of the plates. However, for SUS304/Si3N4 FG plates the first natural frequency values are found to increase for ΔT=100K though it again decreases for ΔT=300K.

For both the FGMs considered, for a particular temperature gradient ΔT and power index value k, the highest value of the first NF is observed for porosity type 2 while the lowest value occurs for porosity type 3. The NF values are found to decrease with increase is the power index values for a particular temperature gradient and porosity type.

3.6 *CONCLUSIONS*

1. For a certain value of the power index k, the maximum value of the first natural frequencies is observed for the untwisted plate (ψ =0˚) and decreases with an increase in the twist angle (ψ). This is due to the fact that the stiffness of the plate decreases with an increase in the twist angle. However, the second natural frequencies are found to increase with an increase in the twist angle of the FGM plate.

2. In case of both twisted and untwisted plates, both the first and second natural frequencies are found to decrease with an increase in the power index value (k) for all the porosity types considered. This is due to the fact that the contribution of the metallic constituents predominates with an increase in the power index value (k) which have lower strength compared to their ceramic counterparts.

3. For all the FGM combinations considered in the present work, the highest values of both the first and second natural frequencies of the FGM plates are observed for porosity type 1 while the lowest value is observed for porosity type 2.

4. For a certain value of the power index k, the maximum value of the first natural frequencies is observed for the square plate (a/b=1) and decreases with an increase in the aspect ratio for all the porosity types. This clear trend of decrease in the natural frequency values is due to the fact that the stiffness of the plate decreases with an increase in the aspect ratio.

5. For a certain value of the power index k, both the first and the second natural frequencies are found to increase with an increase in the non-dimensional rotational speeds (Δ_r) at all the porosity types considered. This increase in the natural frequencies may be attributed to the fact that there is a gradual increase in the structural stiffness of the FGM plate owing to centrifugal stiffening effect with increase in rotation.

6. For Ti–6Al–4V/Aluminium oxide FG plates considered, the first natural frequency values are found to decrease with an increase in the temperature gradient (ΔT) from 0 to 300K for all the power index (k) and porosity types. This is due to the fact that internal thermal strains (negative in nature) are developed inside the FGM plates with temperature rise which results in a decrease in the overall stiffness of the plates.

CHAPTER - IV

REFERENCES

[1] M. Koizumi, 1997, FGM Activities in Japan, Composites Part B: Engineering Volume 28, Issues 1–2, 1997, Pages 1-4

[2] H. Mandal, N Calisackibas, 2006, SiAlON based functionally graded materials, Ceramic-Matrix Composites, Microstructure, Properties and Applications, 2006

[3] Kim J. Kim, K.K. Zur, J.N. Reddy, 2018, Bending, free vibration, and buckling of modified couples stress-based functionally graded porous micro-plates. Compos. Struct. 2019, 209, 879–888.

[4] S. Coskun, J. Kim, H. Toutanji, 2019, Bending, Free Vibration, and Buckling Analysis of Functionally Graded Porous Micro-Plates Using a General Third-Order Plate Theory, Journal of Composite Science, 3, 15

[5] Pradhan, S.C., Loy, C.T., Lam, K.Y. and Reddy, J.N., 2000, Vibration Characteristics of Functionally Graded Cylindrical Shells under Various Boundary Conditions. Applied Acoustics, 61, 111-129

[6] Zhao, X., Lee, Y.Y. and Liew, K.M., 2009, Mechanical and thermal buckling analysis of functionally graded plates. Composite Structures, 90(2), 161-171

[7] Xiao-Lin Huang, Hui-Shen Shen, 2004, Non linear vibration and dynamic response of functionally graded plates in thermal environment, International Journal of Solids and Structures, 41, 9-10, 2403-2427

[8] Alijani, Bakhtiari-Nejad, Amabili, 2011, Nonlinear vibrations of FGM rectangular plates in thermal environments, Composite Structures 93(10):2541–2553

[9] L. X. Peng, S. Y. Chen, D. Y. Wei, W. Chen, Y. S. Zhang, 2022, Static and free vibration analysis of stiffened FGM plate on elastic foundation based on physical neutral surface and MK method, Composite Structures, Volume 290, 15 June 2022, 115482

[10] Phuc Pham Minh, Duong Tuan Manh, Nguyen Dinh Duc, 2021, Free vibration of cracked FGM plates with variable thickness resting on elastic foundations, Thin-Walled Structures, Volume 161, April 2021, 107425

[11] Phuc Pham Minh, Nguyen Dinh Duc, 2021, The effect of cracks and thermal environment on free vibration of FGM plates, Thin-Walled Structures, Volume 159, February 2021, 107291

[12] Gunes R., Aydin M., 2010, Elastic response of functionally graded circular plates under a drop-weight, Composite Structures, 92, 2445-2456

[13] Gunes R., Aydin M., Apalak M.K., Reddy J.N., 2011, The elasto-plastic impact analysis of functionally graded circular plates under low-velocities, Composite Structures, 93, 860-869

[14] Etemadi E., Afaghi Khatibi A., Takaffoli M., 2009, 3D finite element simulation of sandwich panels with a functionally graded core subjected to low velocity impact, Composite Structures, 89, 28-34

[15] XuYalan, QianYu, Gangbing Song, 2016, Stochastic finite element method for free vibration characteristics of random FGM beams, Applied Mathematical Modelling, Volume 40, Issues 23–24, December 2016, Pages 10238-10253

[16] Larson R.A., Palazotto A.N., 2009, Property estimation in FGM plates subjected to low- velocity impact loading, Journal of Mechanics of Materials and Structures, 4, 1429-1451

[17] Larson R.A., Palazotto A., 2006, Low velocity impact analysis of functionally graded circular plates, Proceedings of IMECE2006 2006 ASME International Mechanical Engineering Congress and Exposition, Chicago, Illinois, USA, paper No.: IMECE2006-14003

[18] Wirowski A., 2009, Free vibrations of thin annular plates made from functionally graded material, Proceedings in Applied Mathematics and Mechanics, 9, 261-262

[19] Wirowski A., 2011, Different methods of modelling vibrations of plates made of functionally graded materials, Electronic Journal of Polish Agricultural Universities, 14, 3

[20] Wirowski A., 2012, Self-vibration of thin plate band with non-linear functionally graded material, Archives of Mechanics, 64, 603-615

[21] Giannakopoulos A.E., Suresh S., 1997, Indentation of solids with gradients in elastic properties: part I. Point force, International Journal of Solids and Structures, 34, 2357-2392

[22] Giannakopoulos A.E., Pallot P., 2000, Two-dimensional contact analysis of elastic graded materials, Journal of Mechanics and Physics of Solids, 48, 1597-1631

[23] Mao Y.Q., Fu Y.M., Chen C.P., Li Y.L., 2011, Nonlinear dynamic response for functionally graded shallow spherical shell under low velocity impact in thermal environment, Applied Mathematical Modelling, 35, 2887- 29

[24] Conway H.D., 1956, Analytical model for delamination growth during small mass impact on plates, ZAMP, 7, 80-85

[25] Turner J.R., 1980, Contact on a transversely isotropic half-space, or between two transversely isotropic bodies, International Journal of Solids and Structures, 16, 409-419

[26] Reid A. Larson, Anthony Palazotto, 2006, Low Velocity Impact Analysis of Functionally Graded Circular Plates, ASME 2006 International Mechanical Engineering Congress and Exposition

[27] Shariyat M., Jafari R., 2013, Nonlinear low-velocity impact response analysis of a radially preloaded two-directional-functionally graded circular plate: a refined contact stiffness approach, Composites, Part B: Engineering, 45, 981-994

[28] Shariyat M., Farzan F., 2013, Nonlinear eccentric low-velocity impact analysis of a highly prestressed FGM rectangular plate, using a refined contact law, Archive of Applied Mechanics, 83, 623-641

[29] Khalili S.M.R., Malekzadeh K., Veysi Gorgabad A., 2013, Low velocity transverse impact response of functionally graded plates with temperature dependent properties, Composite Structures, 96, 64-74

[30] Dai H.L., Guo Z.Y., Yang L., 2012, Nonlinear dynamic response of functionally graded materials circular plates subject to low-velocity impact, Journal of Composite Materials, DOI: 10.1177/0021998312458132

[31] Kim J.H., Paulino G.H., 2002, Isoparametric graded finite elements for nonhomogeneous isotropic and orthotropic materials, Journal of Applied Mechanics, 69, 502-514

[32] Zhang Z., Paulino G.H., 2007, Wave propagation and dynamic analysis of smoothly graded heterogeneous continua using graded finite elements, International Journal of Solids and Structures, 44, 3601-3626

[33] Ashrafi H., Asemi K., Shariyat M., Salehi M., 2013, Two-dimensional modeling of heterogeneous structures using graded finite element

[34] Ashrafi H., Asemi K., Shariyat M., Salehi M., 2013, Two-dimensional modeling of heterogeneous structures using graded finite element

[35] Jam J. E., Kiani Y. , 2015, "Low velocity impact response of functionally graded carbon nanotube reinforced composite beams in thermal environment" Composite Structures, 132, 35–43

[36] Malekzadeh P., Dehbozorgi M. , 2016, "Low velocity impact analysis of functionally graded carbon nanotubes reinforced composite skew plates" Composite Structures, 140, 728–748

[37] Selim B.A., Zhang L.W., Liew K.M. , 2017 "Impact analysis of CNT-reinforced composite plates based on Reddy's higher-order shear deformation theory using an element-free approach" Composite Structures, 170, 228–242

[38] Mata-Diaz A., Lopez-Puente J., Varas D., Pernas-Sanchez J., Artero-Guerrero J.A. , 2017, "Experimental analysis of high velocity impacts of composite fragments" International Journal of Impact Engineering, 103, 231-240

[39] Yang S., Chalivendra V. B., Kim Y. K. , 2017 "Fracture and impact characterization of novel auxetic Kevlar/Epoxy laminated composites" Composite Structures, 168, 120–129

[40] Liao B.B., Liu P.F. , 2017, "Finite element analysis of dynamic progressive failure of plastic laminates under low velocity impact" Composite Structures, 159, 567–578

[41] Neogi S. D., Karmakar A., Chakravorty D. , 2017 "Finite Element Analysis of Laminated Composite Skewed Hypar Shell Roof under Oblique Impact with Friction" Procedia Engineering, 173, 314-322

[42] Coelho S.R.M., Reis P.N.B, Ferreira J.A.M, Pereira A.M. , 2017 "Effects of external patch configuration on repaired composite laminates subjected to multi-impacts" Composite Structures, 168, 259–265

[43] Kursun A., Senel M., Enginsoy H. M. , 2015, "Experimental and numerical analysis of low velocity impact on a preloaded composite plate" Advances in Engineering Software, 90, 41-52

[44] Chen Y., Hou S., Fu K., Han X., Ye L. , 2017 "Low-velocity impact response of composite sandwich structures: Modelling and experiment" Composite Structures, 168, 322–334

[45] Kiani Y., Sadighi M., Salami S. J, Eslami M.R. , 2013, “Low velocity impact response of thick FGM beams with general boundary conditions in thermal field” Composite Structures, 104, 293–303

[46] Huang C. Y., Chen Y. L. , 2016, “Design and impact resistant analysis of functionally graded Al2O3-ZrO2 ceramic composite” Materials and Design, 91, 294–305

[47] Zhang J., Li S. , 2010 “Dynamic buckling of FGM truncated conical shells subjected to nonuniform normal impact load” Composite Structures, 92, 2979–2983.

[48] Eghtesad A., Shafiei A.R., Mahzoon M. , 2012, “Study of dynamic behavior of ceramic–metal FGM under high velocity impact conditions using CSPM method” Applied Mathematical Modelling, 36, 2724–2738

[49] Zhang X., Zhang H. , 2013 “Optimal design of functionally graded foam material under impact loading” International Journal of Mechanical Sciences, 68, 199–211

[50] Ding S. H., Li X. , 2013, “The fracture analysis of an arbitrarily oriented crack in the functionally graded material under in-plane impact loading” Theoretical and Applied Fracture Mechanics, 66, 26–32

[51] Damanpack A.R., Shakeri M., Aghdam M.M. , 2013 “A new finite element model for lowvelocity impact analysis of sandwich beams subjected to multiple projectiles” Composite Structures, 104, 21–33

[52] Shariyat M., Nasab F. F. , 2014 “Low-velocity impact analysis of the hierarchical viscoelastic

[53] Johnson A.F., Pickett A.K., Rozycki P., , 2001 “Computational methods for predicting impact damage in composite structures” Composites Science and Technology, 61, 2183–2192

[54] Caputo F., Luca A. De, Lamanna G., Borrelli R., Mercurio U. , 2014 “Numerical study for the structural analysis of composite laminates subjected to low velocity impact” Composites: Part B, 67,296–302

[55] Singh H., Mahajan P. , 2016 “Analytical modeling of low velocity large mass impact on composite plate including damage evolution” Composite Structures, 149, 79–92

[56] R.M. Jones, “Mechanics of Composite Materials”, International Student Edition 1975.

[57] P.C. Yang C.M. Morris and Y. Stavasky, “Elastic Wave Propagation in Heterogenous Plates”, Int. J. Solids and Structures, Vol. 2, (1966), p. 665-684.

[58] Bathe, K.J., Finite Element Procedures in Engineering Analysis, (1990), Prentice Hall of India, New Delhi

[59] Karmakar A. and Sinha P. K., “Failure Analysis of Laminated Composite Pretwisted Rotating Plates”, J. Reinforced Plastics and Composites, 20, No.15, pp.1326-1357, 2001

[60] Bossak, M.A.J. and Zienkiewicz, O.C., Free Vibration of Initially Stressed Solids with Particular Reference to Centrifugal Force Effects in Rotating Machinery, Journal of Strain Analysis, Vol. 8, No. 4 (1973), p. 245-252

[61] Sreenivasamurthy, S. and Ramamurti, V., Coriolis Effect on the Vibration of Flat Rotating Low Aspect Ratio Cantilever Plates, Journal of Strain Analysis, Vol. 16, No. 2 (1981), p. 97-106